

THAT LOOKS ABOUT RIGHT!



UNIVERSITY OF CALIFORNIA
SAN DIEGO

2022-2023

AIAA DESIGN, BUILD, FLY
DESIGN REPORT

TABLE OF CONTENTS

1	Executive summary	2	page
2	Management Summary	4	page
	2.1 Team Organization and Personnel	4	
	2.2 Project Timeline	5	
	2.3 Budget	6	
	2.4 Impact of External Factors	7	
3	Conceptual design	8	page
	3.1 Competition Overview and Scoring	8	
	3.2 Sensitivity Analysis	10	
	3.3 Translation into design requirements	11	
	3.4 Configuration Selection	12	
	3.5 Final Conceptual Design	17	
4	Preliminary design	18	page
	4.1 Overall Design Methodology	18	
	4.2 Propulsion Analysis	19	
	4.3 Fuselage Sizing	23	
	4.4 Wing Sizing	23	
	4.5 Aerodynamic Analysis	23	
	4.6 Stability and Control Analysis	30	
	4.7 Mission Model	31	
5	Detail design	34	page
	5.1 Final Design Parameters	34	
	5.2 Structural characteristics	35	
	5.3 System and subsystem architecture	36	
	5.4 Weight and balance	43	
	5.5 Expected performance	44	
	5.6 Drawing package	45	
6	Manufacturing plan	46	page
	6.1 Investigation of manufacturing processes	46	
	6.2 Assembly method selection	46	
	6.3 Manufacturing timeline	49	
7	Testing plan	50	page
	7.1 Testing Schedule	50	
	7.2 Ground Testing	50	
	7.3 Flight Testing Plan	51	
8	Performance results	53	page
	8.1 Aircraft and Subsystem Performance	53	
	8.2 Flight Performance	55	
	8.3 Future work and concluding remarks	55	
9	Bibliography	56	page

1. Executive Summary

This report, presented by the Design/Build/Fly team at the University of California, San Diego (DBF at UC San Diego), details the team's planned approach for the design, analysis, manufacturing, and testing of an unmanned electric radio-controlled model aircraft for participation in the American Institute of Aeronautics and Astronautics' Design/Build/Fly 2022-2023 competition.

The 2021-2022 year was the first time that any member of the UCSD team went to a competition. Results from last year heavily influenced the preliminary design decisions for this year's competition. The 2022 competition aircraft performed poorly due to far-reaching goals combined with poor scheduling and a lack of experience. This culminated in a plane that attempted to maximize points earned in every mission, but this resulted in a flawed plane that could not even complete any of the missions. The plane ended up crashing in the first mission due to flight instability and was out of commission after receiving irreparable damage.

With this in mind, the team decided on creating a plane for the 2023 competition that could fly all three missions successfully, without attempting to maximize the performance score. This would reduce the complexity of the plane, which in theory, gives the plane more flexibility in case issues arise in design, manufacturing, or flight. Additionally, past competition scores showed that the teams that were able to complete all missions were placed high in the leaderboards.

2. Management Summary

The management summary details the team's organizational structure and members, as well as the schedule and deadlines.

2.1 Team Organization and Personnel

DBF at UC San Diego is organized in a loose hierarchical structure. The team is directed by a project manager and a chief engineer. The project manager is responsible for organization and logistics, including communication with the faculty advisor and other UCSD engineering staff, planning and organizing meetings, securing build and storage space, and ensuring that the team maintains its project schedule. The chief engineer supervises the overall design process and leads the systems-level engineering. These two leading members have the final say in all design decisions and supervise six sub-teams. Each sub-team "lead" directs their respective sub-team, trains new members, and reports to the other lead members at weekly meetings. Non-lead members may be a part of one or multiple sub-teams, and their responsibilities vary between sub-teams. Members of each subteam that are sufficiently trained and motivated can succeed outgoing team members in future years. A visual of the DBF at UC San Diego team structure can be found in **Figure 2.1**.

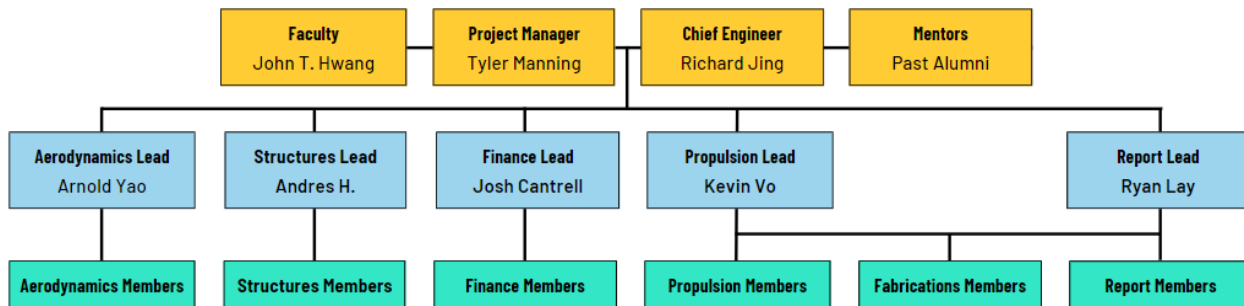


Figure 2.1 • DBF at UC San Diego team structure

Each week, the subteams meet to explore design arrangements, assign tasks, and provide technical assistance to new members. The subteams' leads, project manager, and chief engineer hold weekly meetings to review the results of the sub-team meeting and to make high-level decisions. There are also occasional conferences between the lead members and the faculty advisor regarding design-related issues and reviewing team decisions. DBF at UC San Diego is composed of multiple subteams which are responsible for different aspects of competition plane design and construction: Aerodynamics, Fabrications, Finance, Propulsion, Report, and Structures. These unique roles are detailed in **Figure 2.2** below.

Subteam	Function
Aerodynamics	Designs control surfaces, selects airfoils, and sizes wing and tail to minimize drag.
Fabrication	Orders, builds, and assembles aircraft components; defines manufacturing limitations.
Finance	Handles purchases and expenses, networks with industry, and secures funds.
Propulsion	Conducts thrust stand tests; sizes motor, propeller, and battery to optimize thrust.
Report	Communicates competition rules; writes and edits proposals and reports; compiles data from technical subteams.
Structures	Conducts structural analyses and integrity tests; designs aircraft components and the fuselage.

Figure 2.2 • The list of subteams and their respective responsibilities.

2.2 Project Timeline

A timeline was prepared by DBF at UC San Diego at the beginning of the 2022-2023 competition season at the end of October 2022, around the time of the design proposal. As visualized in Figure 2.3, the project timeline was created to plan four main deadlines for the team's main objectives, which are shown as red bars on the figure. The green bars on the figure describe the planned time frame allocated for each part of the design, fabrication, and testing process. The yellow bars show what times the team actually worked on and made progress on the aircraft.

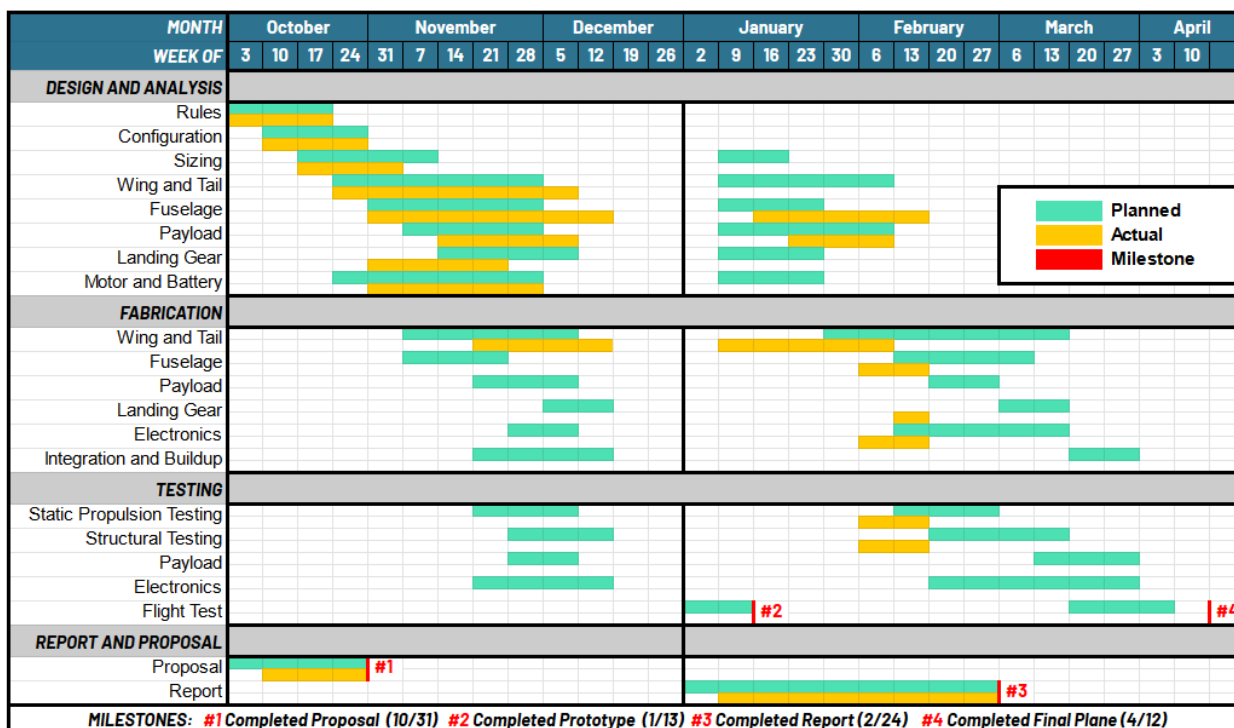


Figure 2.3 • DBF at UC San Diego project timeline.

2.3 Budget

Due to the small size of the plane, as well as an abundance of Foam Core leftover from previous years, it was decided to focus on procuring high-quality composites to manufacture the plane. Due to a malfunction in the team's vacuum pump in the previous year, a new one was ordered to ensure the proper fabrication of the carbon fiber overlay on the four wings.

<i>Fabrications</i>	
Carbon Fiber Sheets 80g / m^2	\$512.00
West System Epoxy	\$106.00
West System Hardener	\$63.00
Epoxy Pumps	\$26.00
Dremmel Guard/Router	\$18.00
Kevlar	\$168.00
Balsa Wood	\$58.00
Carbon Fiber Spar	\$100.00
Spray Adhesive	\$11.00
Tube - Square - Fabric - 0.75 X 0.83 X 66 Inc	\$159.99
<i>Propulsion</i>	
Scorpion SII-4025-330KV	\$569.97
Glacier 30C 4500 mAh 6s 22.2 V Lipo battery	\$103.98
<i>Equipment</i>	
Vacuum Pump	\$850.00
<i>Competition Travel</i>	
Hotels/Lodging	\$1,300.00
Rental Car x2	\$1,000.00
Gas (25mpg, avg \$5 per gallon)	\$372.00
Miscellaneous Costs (tools, materials, last-minute fixes)	\$200
Total Cost:	\$5,617.94

2.4 Impact of external factors

This section is dedicated to explaining the administrative challenges affecting the team's structure in § 2.1 and the team's schedule in § 2.2. Early fall proved challenging for the team's fabrication schedule as the team's build room access was unexpectedly revoked and an application for a new space took time to be processed. This, alongside conflicting designs amongst the technical teams, put a large amount of uncertainty on the overall direction. The design of the wing and motors were completed on schedule, but the rest of the design would not be finalized until mid-February.

November brought another host of issues, the senior lead in charge of fabrications stepped down due to the pressure of graduate school. The former lead would be able to provide technical support, but they would no longer be able to consistently direct the subteam. This caused a major shift in the structure of the team, there was no non-lead member that had the capabilities to take over the vacant role. The disruption in the manufacturing schedule and the confusion of responsibility led to delayed orders of materials, which hampered the team's ability to start the building process. Member retention was also impacted by this event, as many of the subteam's newer members lost interest when the fabrication subteam stopped its work process.

3. Conceptual Design

This section of the report summarizes the first stage of the aircraft design process. Mission requirements and design constraints were identified and a scoring sensitivity analysis was performed. Afterward, design and subsystem requirements were developed to form the basis of an initial plane design.

3.1 Competition overview and scoring

The team's first goal in the conceptual design process is to gain a full understanding of the year's rules and missions. The following subsection provides a summary of the most important points.

The 2023 AIAA DBF competition consists of one ground mission and three flight missions. Each mission, defined by unique scoring parameters, contributes to the team's final score. The report score serves as a multiplier upon the summed mission scores to give the final score **Eq. (1)**.

$$S_{FINAL} = S_{REPORT} \times (S_{GROUND} + S_{M1} + S_{M2} + S_{M3}) \quad \text{Eq. (1)}$$

Assuming that the team and aircraft are able to successfully complete each of the four missions, they will earn a summed mission score between 3 and 8 points, with the report score adjusting it accordingly. The remainder of this report is presented under the assumption that all four missions are successfully executed.

3.1.1 • Ground Mission

For the ground mission, the team's pilot and a designated assembly crew member will have all aircraft components and payloads for the three missions inside a closed shipping box. Before beginning the test, the team will use two coin flips to determine the wing set components which will be used, and the assembly crew member will assemble the aircraft and load the heaviest payload configuration. Within 10 minutes, the assembly crew member must assemble the aircraft, install the structural test fixture onto the wing tips, and apply test weights to the center of the aircraft fuselage. Both the test weights and structural test fixture will later be removed and recorded. Any structural failure or deformation will result in a test failure. The mission will demonstrate the structural margin of the team's aircraft, and the score of which will be determined by the total test weight and the maximum aircraft weight **Eq. (2)**.

$$S_{GM} = \frac{[w_{plane} \div w_{test\ weight}]_{UCSD}}{[w_{plane} \div w_{test\ weight}]_{Max}} \quad \text{Eq. (2)}$$

3.1.2 • Flight Overview

The aircraft will follow an identical path during each flight mission. The path consists of two 1,000-foot straights connected at either end by 180° turns and a single 360° turn in the middle of the downward straight. The take-off field is 60 feet in length, for all flight missions. **Figure 3.1** shows the flight path broken into flight components.

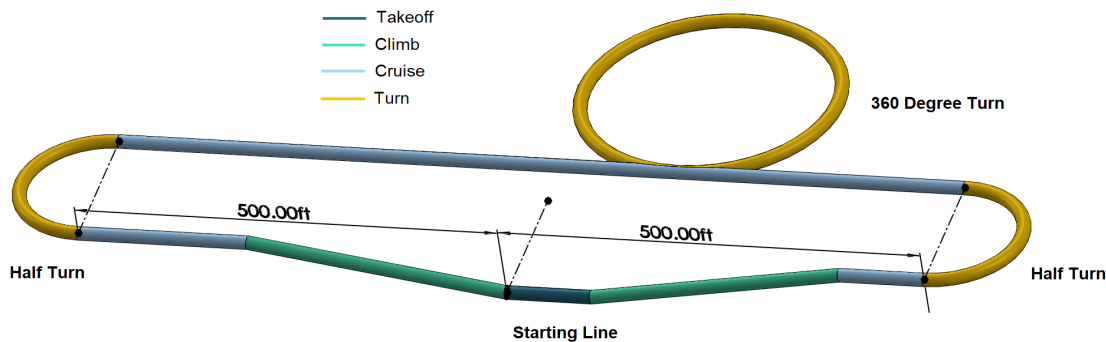


Figure 3.1 • 3-D Model of the AIAA DBF competition flight path

3.1.3 • Mission 1

Mission 1 serves to prove the aircraft's baseline flight capabilities. The team will use two coin flips to determine which wing set to use for the mission, then the aircraft must finish 3 complete laps within the 5-minute flight window. A successful landing that is not part of the 5-minute time window is required to get a score **Eq. (3)**. No payload is carried for Mission 1.

$$S_{M1} = 1 \quad \text{Eq. (3)}$$

3.1.4 • Mission 2

Mission 2 demonstrates the aircraft's ability to fly with a maximized payload in the form of a surveillance electronics package. Two coin flips will be used to determine which wing set components to use for the mission. The team has a 10-minute window to fly the loaded aircraft, and the team's Mission 2 score is a function of the electronics package's weight and the number of full laps completed within the timeframe **Eq. (4)**. A successful landing that is not part of the 10-minute time window is required to get a score.

$$S_{M2} = 1 + \frac{[w_{payload}/L]_{UCSD}}{[w_{payload}/L]_{max}} \quad \text{Eq. (4)}$$

3.1.5 • Mission 3

Mission 3 simulates a jamming flight. Before the flight, the team will use two coin flips to determine which wing set components to be used, and, under the direction of the flight line judge, the team will install the jamming antenna on the side of the aircraft that is opposite to the flight safety line in the direction of takeoff. The team will have a 5-minute window to complete 3 full laps. A successful landing that is not part of the given timeframe is required to get a score. The score will be a function of the Jamming Antenna length and mission time used **Eq. (5)**.

$$S_{M3} = 2 + \frac{[a_{length}/t]_{UCSD}}{[a_{length}/t]_{max}} \quad \text{Eq. (5)}$$

3.1.6 • Design Constraints

The design constraints that were identified by the team through the mission requirements and rules document are summarized in **Figure 3.2**.

Category	Constraint
General	<ul style="list-style-type: none"> • Maximum allowable total length, width, and height is 62 inches • Takeoff field length is 60 feet for all missions • Left and right wings are chosen randomly for each mission
Payload	<ul style="list-style-type: none"> • Package weight equal to 30% of the gross plane weight
Antenna	<ul style="list-style-type: none"> • Fixed to one wing tip, chosen randomly, causes torque
Power Supply	<ul style="list-style-type: none"> • All power for takeoff and flight must be sourced from the aircraft's propulsion system. • Batteries must be either LiPo or NiCad/NIMH. • One battery pack and one battery type allowed • Total stored propulsion energy may not exceed 100 Watt-hours.

Figure 3.2 • Design constraints according to the DBF 2023 Rules.

3.2 Sensitivity Analysis

A scoring sensitivity analysis was developed early in the design process in order to quantify which of the parameters outlined in the scoring equations has the greatest impact on the overall score. The model, designed in MATLAB, considers six variables: report score, the number of laps flown in Mission 2, the package weight for Mission 2, the antenna length for Mission 3, the flight time for Mission 3, and the Ground Mission score. By adjusting the value of one parameter while keeping others constant, the team was able to identify the impact of each individual variable on the total score.

The team has utilized data from previous competitions in order to generate best-guess baselines for the model (Figure 3.3); namely, the team has used scoring data from previous cargo-based competitions to calculate the average score, with the assumption that the score is above zero. Then, by preemptively judging the team's capabilities at the start of the year, the team made the assumption that they would be able to score at least the average.

Variable	Initial Guess
Report Score	0.8
Num. of Laps in M2	3
Antenna Length	4 in.
Package Weight	2.1 lbs
GM Score	Average of past years
M3 Time	180s

Figure 3.3 • Initial best-guess scoring estimate.

In this year's competition, the scoring parameters only lightly affect the total score (Figure 3.4). The parameters for antenna length, number of Mission 2 laps, package weight, and the ground mission score all affected the score similarly. They did not change the total score by more than half a point despite a 50% change in the parameter value. The most significant parameter was the report score, which vastly exceeds the other parameters in terms of the score-to-parameter change ratio. The second-most important parameter was the Mission 3 completion time, but it only changed the total

score by 0.6. Based on these conclusions, accounting for the team's lack of experience and the previous year's challenges, it was decided that the report score and the guarantee to fly all three missions are to be prioritized. By optimizing for higher failure margins, the team could mitigate mistakes in the fabrication process, even if the plane's capabilities ended below its predicted values.

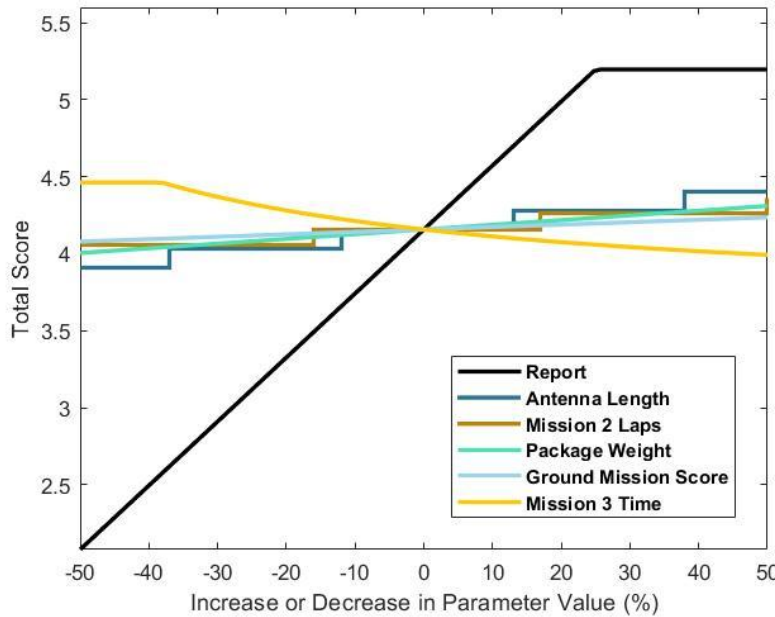


Figure 3.4 • Impact of each scoring parameter on the overall competition score.

3.3 Translation into design requirements

With the sensitivity analysis complete, the team was able to better identify the design choices that would allow the aircraft to perform well in the competition.

3.3.1 • Fuselage

The fuselage needs to have the capacity to hold the electronics and the package, but could otherwise be minimized to reduce weight, as no scoring parameters are related to variable carrying capacity. The integrity of the fuselage needs to withstand a large relative mass, as provided in the Mission 2 parameters.

3.3.2 • Wing and tail

Mid-flight stability is to be prioritized heavily to compensate for the team's lack of experience in piloting and for the completion of Mission 3. To do this, it is necessary to identify an optimal airfoil, wing sizing, and tail sizing combination for the expected weight.

3.3.4 • Propulsion system

According to this year's doctrine, the team decided that it was not required to have a competitive speed. Additionally, the plane was only allowed one battery pack. With this in mind and the fact that both Mission 2 and 3 require increased loads, the team prioritized endurance above speed.

3.3.6 • Other design considerations

A proper landing gear system, robust enough to survive multiple landings, was identified as an important aircraft component.

The low impact of the mission parameters as well as the team's inexperience in fabrications led to a priority for the ease of manufacturing.

3.4 Configuration Selection

Figure 3.5 below provides a summary of the most important design considerations identified in the previous subsection. The team assigned each of the five figures of merit a weight from 1× (least important) to 5× (most important). The requirements are ranked in order of importance from top to bottom and provided the basis by which designs were considered.

Figure of merit	Weight	
Manufacturability	5×	Low manufacturing complexity; cheap, or not time-consuming
Control / Stability	3×	Greater control during maneuvers and steady flight
Aerodynamics	3×	Related to higher endurance, speed, or lift
Structural Strength	3×	Related to improved integrity, prevents breakage
Carrying Capacity	1×	The ability to hold and carry a payload

Figure 3.4 • The team's design considerations, ranked in order of importance

Manufacturability was deemed the most important design parameter and played a considerable role in the team's decisions throughout the decision process. The previous plane's faults as well as the mission parameters' low impact on the score gave confidence to the decision to make the ease of fabrication the highest priority. Later, the resignation of the senior fabrications lead put immense strain on the manufacturing process.

Control and stability were given moderate priority primarily due to the challenge of torque presented in Mission 3. Additionally, Mission 2 will increase the weight of the plane by thirty percent, which will lead to a major disruption in the aircraft's stability if not properly accounted for.

Aerodynamics heavily affects the aircraft's velocity, efficiency, and mission completion time. While generally important for capable flight, it received moderate priority due to the limits of one battery, and the increased load in Mission 2.

Structural strength determines the safety of the aircraft's mounts, fixtures, and fuselage. This consideration was generally important for the aircraft's ability to withstand flight and landings. It received moderate priority because of the need for an antenna mount and the housing for the small container in Mission 3.

Carrying capacity was inherent to Mission 2, but given the fixed and small size of the payload, it was deemed to have the lowest priority compared to the other parameters.

3.4.1 • Aircraft Type



Design Consideration	Weight	Monoplane	Biplane	Flying Wing
<i>Manufacturability</i>	5	5	3	2
<i>Control and Stability</i>	3	4	5	3
<i>Aerodynamics</i>	3	3	2	4
<i>Structural Strength</i>	3	3	4	2
<i>Carrying Capacity</i>	1	3	5	3
Total		58	53	40

Figure 3.5 • Figure of merit matrix for the aircraft type.

Manufacturability was the most important design parameter this year. The team chose the monoplane due to its simplistic design, allowing for the best manufacturability. Closely considered was the biplane, which boasted superior stability and carrying capacity. However, the competition required two sets of wings, which would force the team to create four wings in order to outfit a biplane. Combined with the high price of the team's composite layup, this design was disregarded. The flying wing was disregarded nearly from the start. If built properly, this design would have the best speed and thrust to power efficiency. Unfortunately, the team did not have the expertise to effectively build this design nor the manpower to research the steps to do so. Additionally, speed was not a priority for the team, as our goal was to complete all three missions before competing for standing amongst the top rankings.

3.4.2 • Wing Placement



Design Consideration	Weight	High-Wing	Mid-Wing	Low-Wing
<i>Manufacturability</i>	5	3	4	3
<i>Control and Stability</i>	3	3	3	4
<i>Aerodynamics</i>	3	3	4	2
<i>Structural Strength</i>	3	3	4	3
<i>Carrying Capacity</i>	1	4	3	5
Total		46	55	47

Figure 3.6 • Figure of merit matrix for the wing placement.

In terms of manufacturability, the mid-wing was able to beat both the high-wing and low-wing. For the competition, the wing was required to be split into halves. This prevented the high-wing and low-wing to be built as one piece, nullifying one of their main advantages in manufacturability over the mid-wing.

Additionally, using a mid-wing would allow for the connection points to be attached inside the fuselage, which would increase the moment of the control surfaces as they would be further away from the center of mass. Both the low and high-wing designs have superior carrying capacity, but those factors were disregarded due to the fixed and relatively small size of the payload in Mission 2. Furthermore, the proposed mid-wing's fastening method was deemed to be the most feasible for the team's inexperienced fabrications.

3.4.3 • Wing Shape



Design Consideration	Weight	Rectangular	Tapered	Elliptical	Swept
<i>Manufacturability</i>	5	5	3	1	1
<i>Control and Stability</i>	3	3	4	5	4
<i>Aerodynamics</i>	3	3	4	5	4
<i>Structural Strength</i>	3	4	4	3	2
<i>Carrying Capacity</i>	1	—	—	—	—
Total		61	51	44	29

Figure 3.7 • Figure of merit matrix for the wing shape.

A Wing's shape affects the control and speed of the aircraft. While elliptical and swept wings each have their own niches, they were almost immediately eliminated from consideration due to their high manufacturing complexity. A tapered wing was also considered, as the team had made one in a prior competition, but it was eventually decided that attempting to create two sets of tapered wings would induce too much strain on fabrications. In the end, the team went with the rectangular wing, in large part due to its low manufacturing complexity. Additionally, a rectangular wing would provide greater structural strength, covering for minor mistakes in the fabrication process.

3.4.4 • Empennage

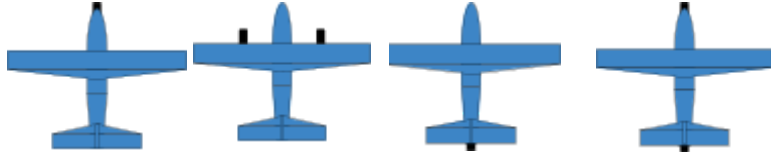


Design Consideration	Weight	Conventional	T-Tail	Cruciform
<i>Manufacturability</i>	5	4	4	3
<i>Control and Stability</i>	3	4	4	4
<i>Aerodynamics</i>	3	4	3	2
<i>Structural Strength</i>	3	4	3	4
<i>Carrying Capacity</i>	1	4	5	5
Total		59	55	50

Figure 3.8 • Figure of merit matrix for the empennage.

The tail plays an important role in keeping the plane level in flight and resisting gusts of wind that could knock it off course. The cruciform tail was considered but quickly discarded from the deliberation, as it was a design that covered the same role as the T-tail, with the exception of higher manufacturing difficulty. Both the T-tail and the conventional tail would have equal manufacturing burdens, as they are both created similarly, with one being the inverse of the other. The T-tail was considered primarily due to its ability to avoid the wake turbulence created by the propeller, allowing for a more stable flight at slow speeds. However, the T-tail also suffers from an increased chance to deep stall, which can occur at a certain angle when the wings cover the airflow to the tail. The UCSD DBF 2021-2022 plane was thought to have crashed in part due to this type of failure. This led to the team deciding on the conventional tail design, despite the disadvantage of turbulent wake.

3.4.5 • Propulsion System



Design Consideration	Weight	Tractor	Dual Tractor	Pusher	Tractor-Pusher
<i>Manufacturability</i>	5	5	3	2	1
<i>Control and Stability</i>	3	3	4	3	2
<i>Aerodynamics</i>	3	3	5	4	5
<i>Structural Strength</i>	3	4	2	2	1
<i>Carrying Capacity</i>	1	3	4	3	2
Total		58	52	40	31

Figure 3.9 • Figure of merit matrix for the propulsion system.

Regarding propeller configurations, the team has considered the conventional tractor propeller and the pusher propeller. A tractor propeller is excellent for balancing the structural load and is decently stable in air and on the ground. However, such a propeller will also create turbulence against the wing sections behind it and reduce the lift generated by the wings. A pusher propeller, on the other hand, combats this issue as its suction of the air reduces turbulence and enhances the lift from the wings. Unfortunately, having a pusher propeller also risks the chances of a sudden stoppage at take-off because the propeller is backward from the center of mass, and the propeller will rotate down toward the ground. The chosen tractor design does not have the problem of induced turbulence on wings and does not suffer from issues with propeller placement. Compared to the push propeller design, the single tractor design is less aerodynamic, but it has significantly greater structural stability and manufacturability, especially considering the single battery limitation. Additionally, with the aircraft being relatively lightweight for a cargo mission, as the fuselage will be smaller in accordance with smaller cargo volume, the batteries will not drain as fast as the dual tractor design will.

3.4.6 • Fuselage Form

<i>Design Consideration</i>	<i>Weight</i>	<i>Square</i>	<i>Rounded Square</i>	<i>Elliptical</i>	<i>Circular</i>
<i>Manufacturability</i>	5	5	5	3	3
<i>Control and Stability</i>	3	2	3	3	4
<i>Aerodynamics</i>	3	2	3	4	5
<i>Structural Strength</i>	3	5	3	1	2
<i>Carrying Capacity</i>	1	3	4	4	4
<i>Total</i>		63	70	54	64

Figure 3.10 • Figure of merit matrix for the fuselage form.

The shape of the fuselage cross-section greatly affects the characteristics of the aircraft. When determining the desired cross-sectional shape, the team weighed the effects of the most popular fuselage shapes on the manufacturability, control and stability, aerodynamics, structural strength, and carrying capacity of the aircraft. A square fuselage minimizes manufacturing difficulties, but generates the highest amount of drag and introduces high stress concentrations at the edges, limiting structural strength. Elliptical and circular fuselage cross sections reduce the aforementioned concerns, but at the cost of greater difficulty in manufacturing, as well as a reduced total cargo area. The compromise that attempts to address both sets of concerns is therefore a rounded square cross-section, as it maintains a relatively low difficulty of manufacturing and high cargo area, while also reducing drag and distributing stress.

3.4.7 • Landing Gear

<i>Design Consideration</i>	<i>Weight</i>	<i>Tricycle</i>	<i>Tip Tricycle</i>	<i>Tail Dragger</i>
<i>Manufacturability</i>	5	3	3	4
<i>Control and Stability</i>	3	4	2	3
<i>Aerodynamics</i>	3	4	1	5
<i>Structural Strength</i>	3	4	2	5
<i>Carrying Capacity</i>	1	4	2	3
<i>Total</i>		55	32	62

Figure 3.11 • Figure of merit matrix for the landing gear.

The choice of the landing gear was determined by the same criteria as the fuselage shape. An ideal landing gear ensures a soft landing while not hampering the stability or aerodynamic performance of the aircraft. A tail dragger landing gear configuration was chosen over a tricycle or tip tricycle configuration as it was the easiest to manufacture, while also outperforming the other designs in terms of aerodynamic performance and structural integrity. The reduced control and stability caused by the tail dragger configuration were not a major concern, as the mid-wing design of the aircraft provides an increased level

of stability. The reduced carrying capacity was also not a major concern due to the smaller payload requirements of this year's competition.

3.5 Final Conceptual Design

The team chose to design a monoplane with a rectangular mid-wing, a conventional tail, a dual tractor propulsion system, a rounded-square fuselage, a tail dragger landing gear setup, and a motor-string cargo storage system that feeds into a scissor-lift deployment mechanism. An early CAD model is shown below in **Figure 3.12**.

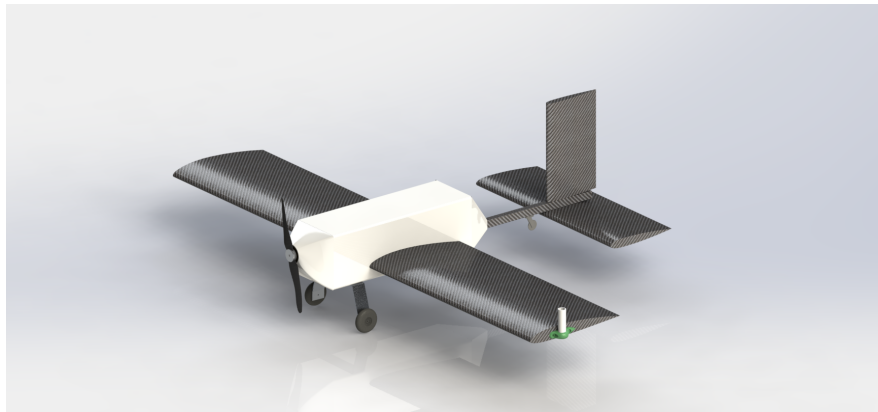


Figure 3.12 • CAD rendering of the aircraft with selected configurations.

4. Preliminary Design

This section describes the team's design methodology, the trade studies and analysis that the team performed, and the expected performance results that the analyses produced.

4.1 Overall Design Methodology

DBF at UC San Diego determined the conceptual design of the aircraft by analyzing the scoring parameters, performing a sensitivity analysis, and identifying the optimal design configurations, as described in § 3.

The team then performed various aerodynamic and propulsion trade studies in order to determine the optimal choice of motor, propeller, wing size, and airfoil. The team also developed estimates of the aircraft's lift, drag, and stability characteristics in flight. Subteams that were responsible for performing these analyses reported to the remainder of the team with their findings, and the team worked together to address design constraints and reach satisfactory compromises. The most crucial design considerations—namely carrying capacity, stability, and manufacturability—formed the basis on which design decisions were ultimately made.

Additional analyses that focused on weight balancing and structural strength, along with input from the fabrications team, either confirmed or rejected the plausibility and effectiveness of each proposed design. Through this process, the team iterated over multiple subsystem designs, including wing and tail sizing, fuselage structure, and deployment mechanism, until it was determined that the aircraft and each composing subsystem would be capable of achieving the team's overall objective. The aerodynamics and propulsion subteams tend to drive the decisions made by the structures and fabrication subteams, but the design process is interwoven between subteams at all steps, as shown in **Figure 4.1** in a simplified manner.

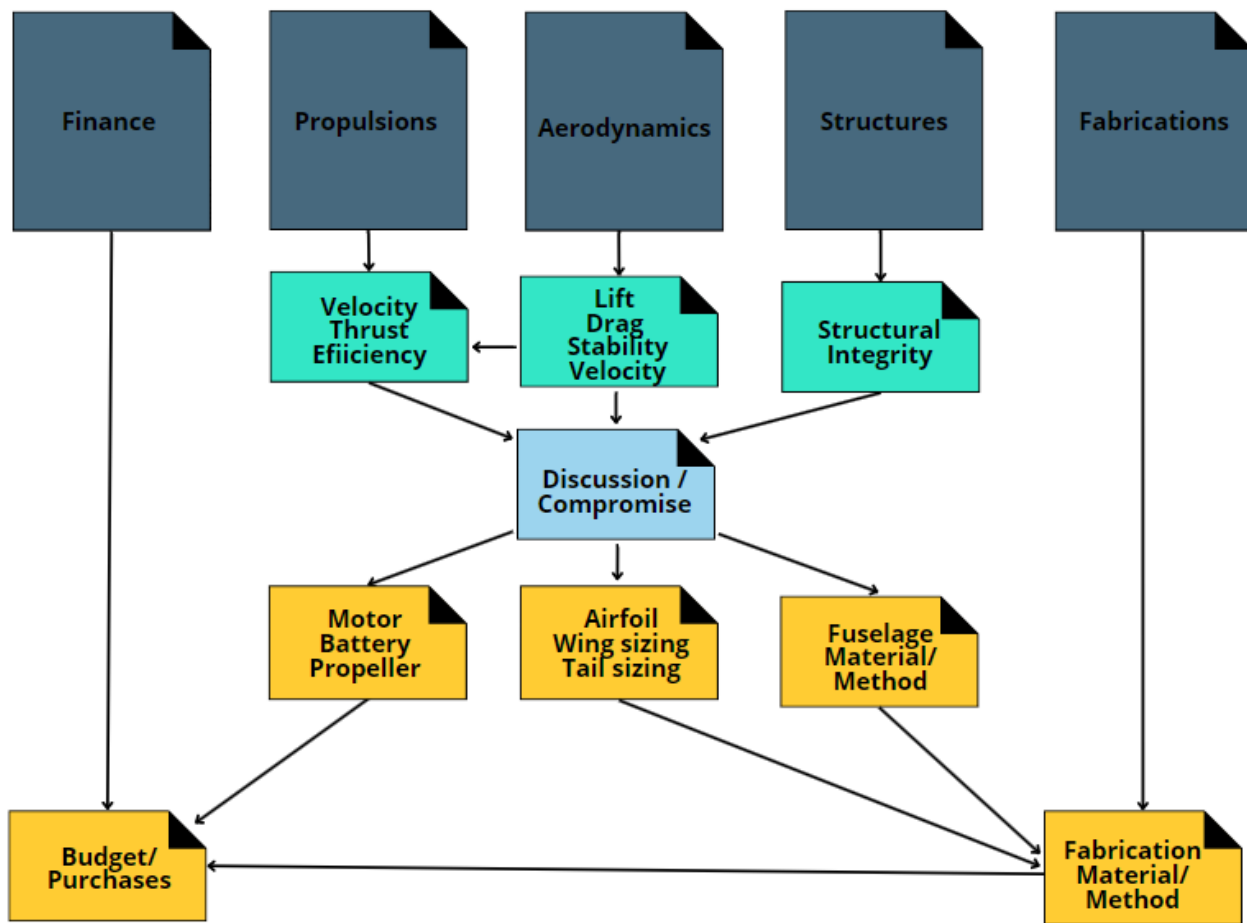


Figure 4.1 • A summary of the team's design process for the 2022-2023 year.

4.2 Propulsion Analysis

In order to estimate the best combination of batteries, motors, and propellers for airspeed requirements set by the aerodynamics subteam, the propulsion subteam utilized an optimization script coded in MATLAB. This script would calculate and compare the net efficiency values of many different propeller and motor combinations and select the configuration that is the highest. A flowchart detailing all aspects of the code is summarized in **Figure 4.2**. Thus, our code optimizes for a configuration with high net efficiency, which is calculated using **Eq. (6)**, and low current draw. The multidisciplinary design optimization problem (MDO) written by Hwang et al. at the University of California, San Diego was used as reference material to create our code [1]:

$$\eta_{net} = \eta_{prop} \times \eta_{motor} = \frac{U_x T}{VI} \quad \text{Eq. (6)}$$

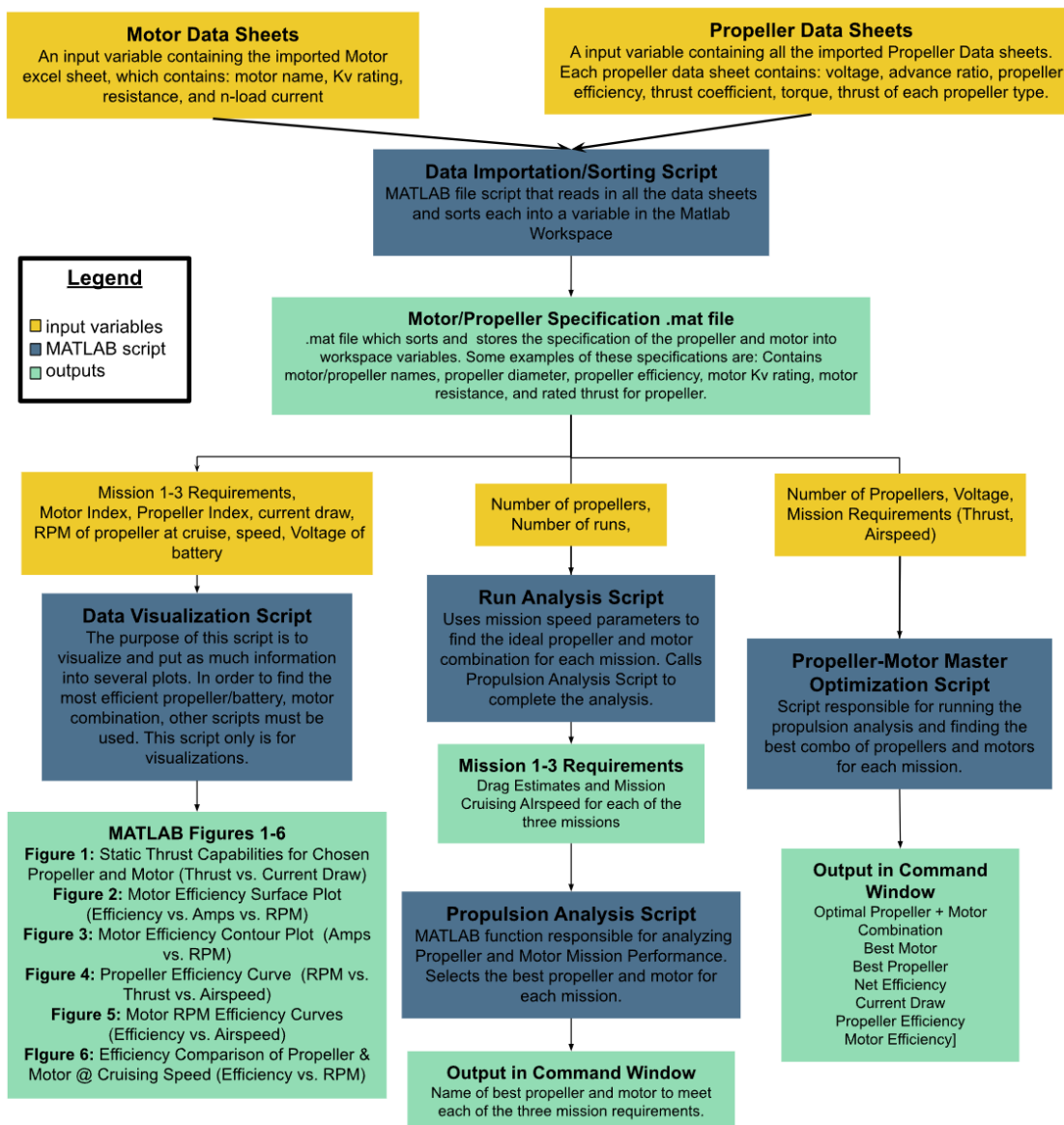


Figure 4.2: This flow chart shows all of the MATLAB files and the input and output files associated with the team's efficiency optimization script. By using our optimization script, our team can make a more informed decision on what parts to include in our propulsion system.

Assuming that airspeed and thrust do not change in the case of steady-level flight and neglecting voltage decay and loss in the battery during flight, the minimization of current draw optimizes for high net efficiency. Thus, our team expects that a configuration with the lowest current draw will result in a longer endurance flight and thus an increase in the aircraft's performance during a mission.

Battery performance data from several hobby store websites, motor performance data from Bunge at Stanford University [2] and Scorpion documentation [3], and propeller performance data from Advanced Precision Composites (APC) [4] were incorporated into our code in order to decide which propeller and motor combinations best meet the mission goals and requirements. This year, the propulsion subteam of

our team accumulated over 250 propeller datasheets and 50 motor data sheets in hopes of improving our script's accuracy. Over 20,000 different propulsion system combinations were iterated through using our optimization scripts based on given mission requirements.

Our code ended up giving different optimal propeller and motor configurations for each of the three missions. For Mission 1, the optimal configuration was a 12x14 propeller and a 190Kv Scorpion SII-5535 motor while the optimal configuration for Missions 2 and 3 was a 12x10E propeller paired with a 330Kv Scorpion SII-4025. Since our team did not want to change the propulsion system in between missions, given that our team is already swapping wings after every flight, we went with the propulsion system that would encompass the requirements of most missions. As such, the team chose a 12x10E APC propeller and 330Kv Scorpion-4025 as the propulsion system for all missions. **Figure 4.3** documents the final configuration chosen by our team. After selecting the motor, finding the right battery for it was not as difficult for us as it was last year. We chose the Glacier 30C 6S battery because it not only met the 100-watt-hour design limit, but we already had a few lying around our build space from previous competitions.

Component/Parameter	Optimal M-1	Optimal M-2	Optimal M-3
<i>Battery Specifications</i>		Glacier 30C 6S 4500 mAh, 22.2 V, lithium-polymer	
<i>Motor Specifications</i>		Scorpion SII-4025 330 Kv	
<i>Propeller, from APC</i>		12 in. x10E in.	
W_{prop}	<i>Propulsion System Weight</i>	36.3 oz	
η_{net}	<i>Net Efficiency at Cruise Conditions</i>		0.82

Figure 4.3 • Chosen propulsion configuration for all missions.

Further trade studies were conducted to verify the chosen motor and propeller through visualization of its performance at the expected cruise velocity, RPM, and current draw, which were all acquired from previous studies. Figures 4.c and 4.d provide two alternate perspectives of propeller performance while figure 4.e shows propeller efficiency. According to the graphs generated by our data visualization script, the theoretical aircraft performs at or near the maximum possible efficiency, which confirms the team's choice of propulsion system.

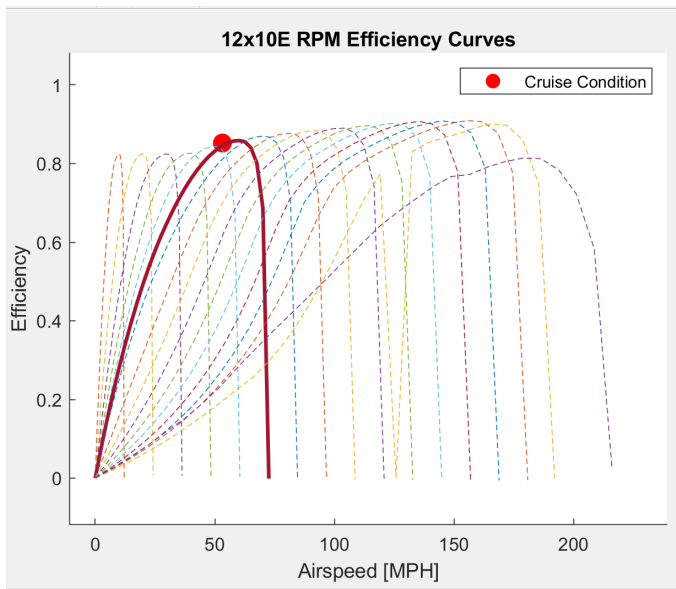


Figure 4.4 • A 2D MATLAB graph plotting the efficiency of the chosen 12x10E propeller. Each curve represents a different RPM value. The chosen configuration is shown in red.

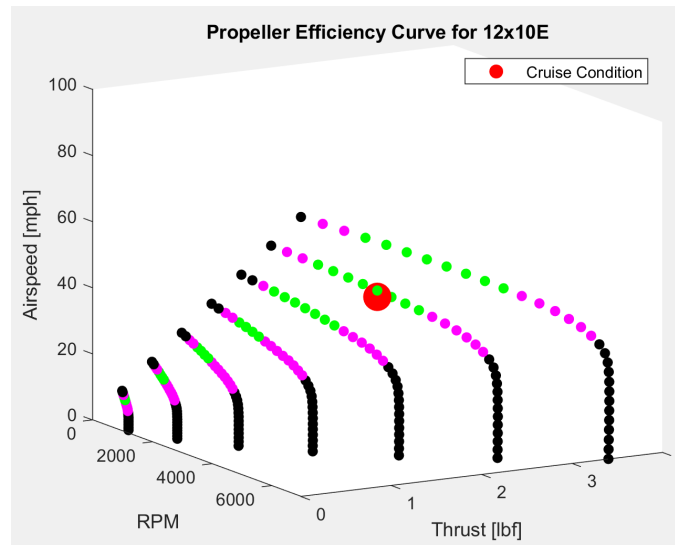


Figure 4.5 • A 3D MATLAB plot showing the relationship between RPM, thrust, and airspeed within propeller efficiency curves for 12x10E propellers.

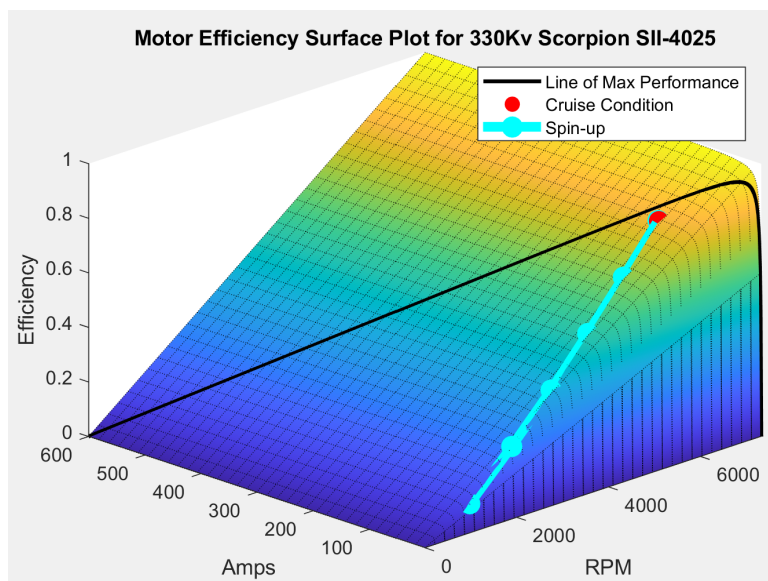


Figure 4.6 • A 3D MATLAB surface plot visualizing the efficiency of the chosen propeller along with current draw and RPM during spin-up and cruise, relative to the line of maximum possible performance.

4.3 Fuselage Sizing

The fuselage was primarily sized to incorporate the fixing structure for the wing mounts, as well as the payload for Mission 2. The relatively small size of the payload (minimum 3" x 3"x 6") for Mission 2 allowed for a proportionately small fuselage, which would help reduce weight and improve the endurance of the plane. Room would also need to be allotted for the avionics and battery which would be placed closer to the nose of the plane. The placement can be seen in § 5. The team eventually agreed upon a fuselage sized at 24 inches in length, 5 inches in width, and 5 inches in height.

4.4 Wing Sizing

This year the team decided to incorporate the 54-inch wingspan for a variety of factors. This is because the plane will be smaller and lighter compared to last year's plane. Additionally, the competition guidelines set a maximum wingspan of 60 inches. These factors caused the team to reduce the wingspan from 72 inches to 54 inches. Additionally, the weight of the plane decreased such that the aircraft such that the wingspan also had to decrease.

$$C_L = \frac{L}{\frac{1}{2} \rho V^2 S} \quad \text{Eq. (7)}$$

A major factor in deciding the wing size was the consideration of the coefficient of lift **Eq. (7)**. **Eq. (7)** describes the lift coefficient C_L with respect to lift force L , air density ρ , plane velocity V , and wing surface area S . By setting a limit and changing several choice parameters, the team was able to calculate an optimal wing size. The estimated sizing parameters are a maximum gross weight of 7 lbs and an airspeed of 85 ft/s. The maximum limit for the wing loading or the maximum weight over the wing area, used by the team was 2.41 lb/ft². By applying **Eq. (7)** to these values, the team calculated an operating lift coefficient of 0.28 corresponding to the maximum wing loading limit. A wing area of 2.91 ft² was calculated from the desired wing loading. Combined with the chosen wingspan of 54 inches, the team determined a chord length of 11.5 inches. A taper ratio of 1 was chosen for the wing design due to manufacturing constraints.

4.5 Aerodynamic Analysis

The team relied on a computational fluid dynamics (CFD) program called XFLR5 to analyze the performance of the airplane. The program provided the non-dimensional coefficients of lift, drag, and moment at various speeds. Since XFLR5 is known to underestimate drag, a component-wise drag build-up method was utilized to enhance the performance analysis.

4.5.1 • Airfoil Selection

The team obtained airfoil data from thousands of airfoils which were inputted into MATLAB. The airfoil has constraints such as that the thickness cannot be greater than 10% of the chord length due to manufacturing processes. The plane cruise condition is at C_L of 0.28. Based on the data from MATLAB, ClarkY, SD 7062, NACA 2412, and the E216 were the top contenders for the airfoil selection. These

airfoils were analyzed on XFLR5 software to determine the optimum airfoil used on the wing with the criteria of minimizing the drag and maximizing the lift. XFLR5 will produce more accurate estimations of the performances of the airfoils. The analysis of XFLR5 was done for a fixed-weight, finite-wing plane. Continuing, the magnitude of induced drag– or the resultant drag created by the presence of lift– is known to be quadratically proportional to the lift coefficient; it also is inversely related to the aircraft wing's aspect ratio and the Oswald efficiency factor $C_{D,i} = \frac{C_L^2}{\pi e AR}$. The document by Sholz suggests that the Oswald efficiency factor relies on the total number of engines and the wing's aspect ratio, taper ratio, and thickness-to-chord length ratio shown in **Eq. (8)**.

$$e = \frac{1}{(1 + 0.12 M^6)[1 + 0.142 + f(\lambda)AR(\frac{10t}{c})^{0.33} + \frac{0.1(3N_e + 1)}{(4 + AR)^{0.8}}]} . \quad \text{Eq. (8)}$$

From XFLR5, the team analyzed the different graphs that were produced. Our goal for the competition was to maximize efficiency. Efficiency is also known as C_L/C_D . The C_L/C_D graph that was produced for the E216 airfoil gave an efficiency that did not meet the team's expectations. The C_L was too high, and a C_L value that is too high will cause the airplane to stall during flight. The SD 7062 Airfoil had the lowest C_L/C_D ratio, which is clearly not optimal for our plane. The numbers and graphs that the XFLR5 programs produced for the Clark Y airfoil impressed the team. The C_L/C_D for the Clark Y airfoil was close to our target value. However, the reason why this airfoil was not chosen is because of its angle of attack. The angle of attack was a little too high for the team's liking. Our aircraft can not afford to have a high angle of attack because a high angle of attack will decrease the amount of lift the aircraft produces. Conversely, a decrease in lift will increase the drag and eventually the aircraft will stall. Because of these reasons, we could not choose the Clark Y airfoil. Based on the XFLR5 analysis, NACA 2412 was chosen due to the airfoil having the highest efficiency CL/CD ratio at 28 at an angle of attack of 2.7° which is shown with the light green curve. An angle of attack of 2.7° is optimal for our aircraft, and with the CL/CD ratio that is given, our team concluded that when in flight, the aircraft will be able to perform to its best ability.

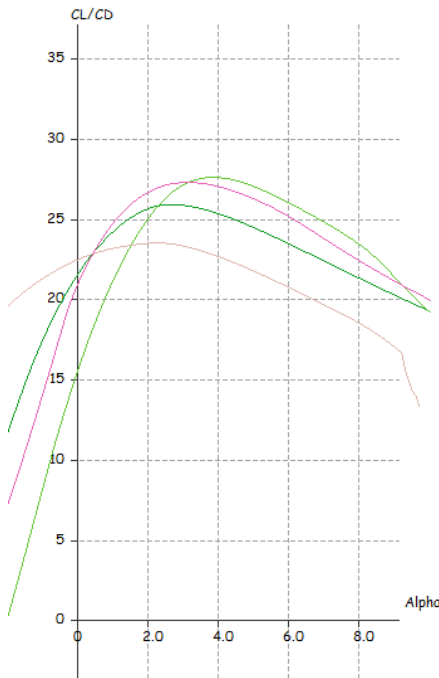


Figure 4.7 • CL/CD vs α generated for a handful of airfoils at cruise conditions.

4.5.2 • Lift Analysis

This year our team used XFLR5 to calculate the overall lift performance of the aircraft. This program was able to perform very precise interpolation along with providing good estimates of the plane's performance with the exclusion of the drag estimations. The wing, which provides the majority of the lift for the aircraft, is what the team performed analysis on (**Figure 4.8**).

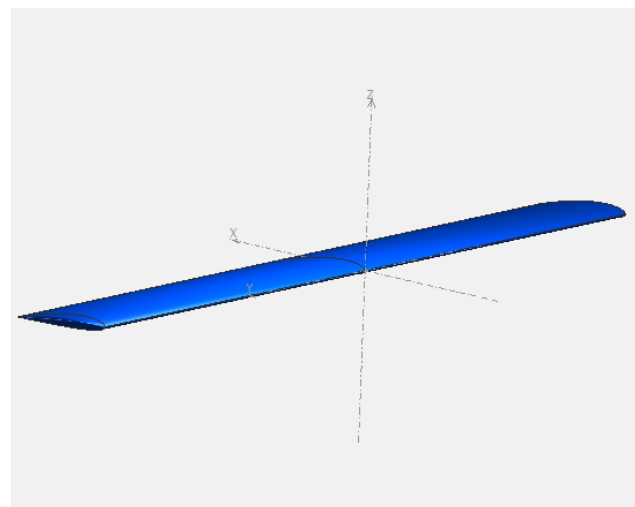


Figure 4.8 • Model of the wing in XFLR5

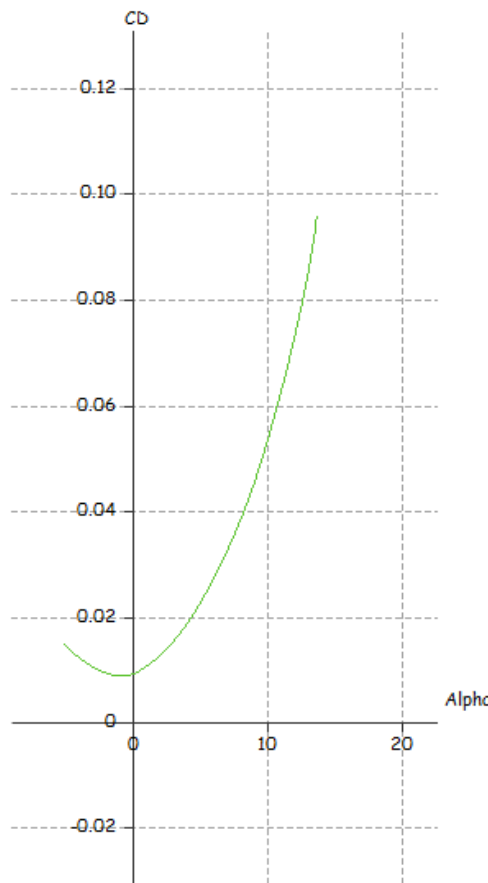


Figure 4.9 • Drag coefficient vs angle of attack

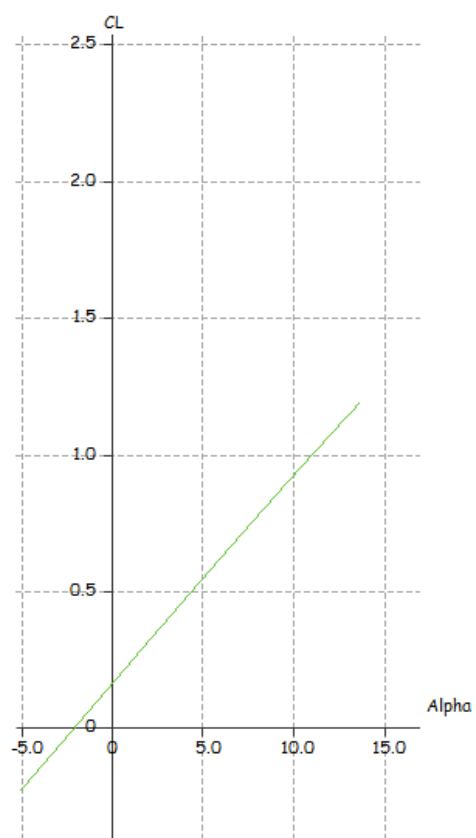


Figure 4.10 • Lift coefficient vs angle of attack

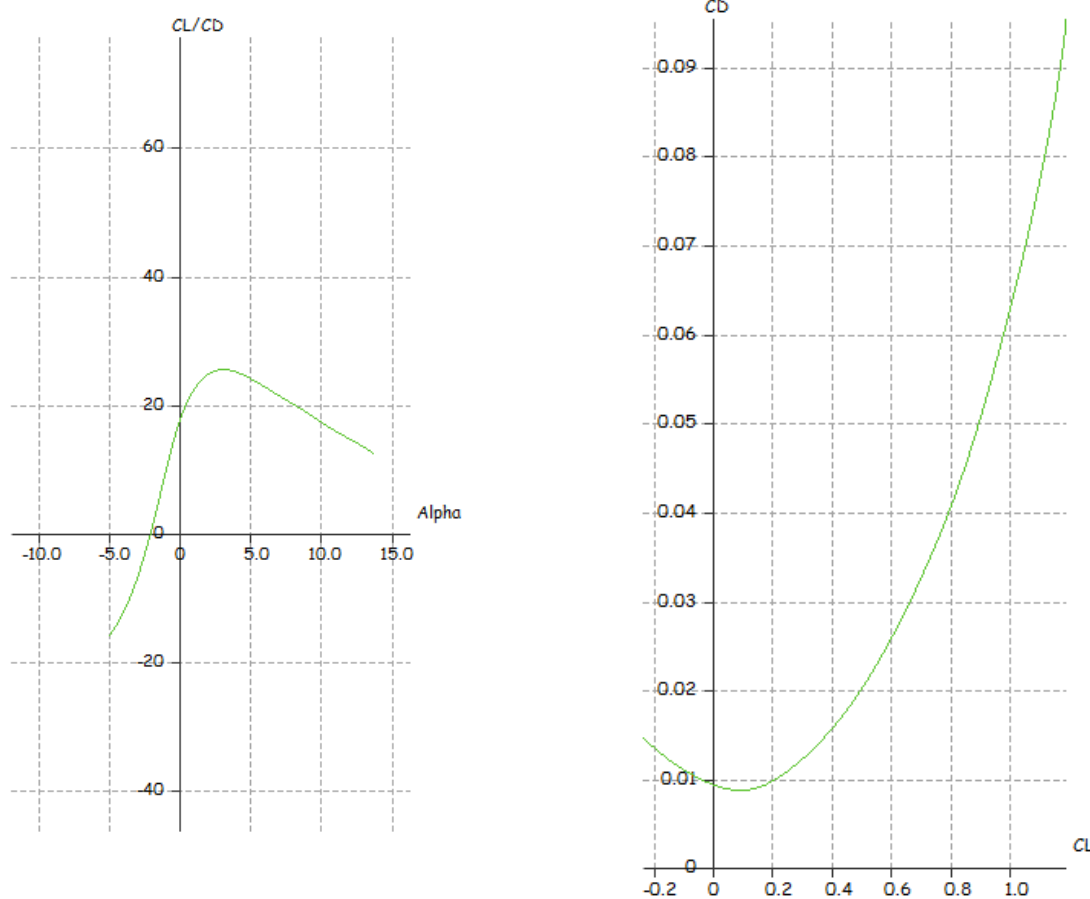


Figure 4.11 • Efficiency vs angle of attack

Figure 4.12 • Drag coefficient vs. lift coefficient

As shown in **Figure 4.10**, an angle of attack at 10° should yield a maximum lift coefficient of 1. Due to some limitations of XFLR5, it was unable to interpolate and produce more data points when it comes to higher lift coefficients at higher angles of attack, so it is safe to say that the maximum lift coefficient in our data is not the highest that we could achieve. According to **Figure 4.11**, our optimal efficiency (C_L/C_D) is roughly 27.5, at an angle of attack of 3.7° which can be assumed to be our climb angle. When it comes to calculating drag, XFLR5 is notoriously known to underestimate drag, which could lead to a discrepancy in the data in **Figures 4.9, 4.10, and 4.12**, meaning that our C_D value could be higher which overall lowers the value of our (C_L/C_D) efficiency. Despite the underestimation of the C_D , the data produced should yield a close enough approximation. Using XFLR5, we were able to obtain the maximum stall angle along with the maximum lift coefficient, and from that, we were able to calculate the stall velocity using the lift coefficient equation from **Eq. (7)**.

Condition		Mission	Angle of attack	Lift Coefficient	Velocity
CR	Cruise Conditions	M-1	2.8°	0.28	60 ft/s
		M-2	2.8°	0.28	85 ft/s
		M-3	2.8°	0.28	85 ft/s
ST	Stall conditions	M-1	13.6°	1.18	36.6 ft/s
		M-2	13.6°	1.18	46.6 ft/s
		M-3	13.6°	1.18	46.6 ft/s
TO	Takeoff condition Flaps down at 25°	M-1	0°	0.495	56.5 ft/s
		M-2	0°	0.495	63.2 ft/s
		M-3	0°	0.495	63.2 ft/s

Figure 4.13 • Angle of attack, lift coefficient, and velocity at various flight conditions

4.5.4 • Drag Analysis

The XFLR5 program tends to underestimate the drag produced such that the drag needs to be manually calculated with the equation derived by professor Dieter Sholz at the Hamburg University of Applied Sciences. Smaller contributions to drag—such as flap, slat, gear, wave, and the antenna drag—were neglected, leaving the parasitic and induced drag produced by the main aircraft fixtures to be calculated.

We began by computing the parasitic drag, as given by the following equation:

$$C_{D,0} = \sum_{c=1}^n C_{f,c} \cdot FF_c \cdot Q_c \cdot \frac{S_{wet,c}}{S_{ref}} + C_{D,other} \quad \text{Eq. (9)}$$

Within Eq. (9), $C_{f,c}$ is the skin friction drag coefficient, FF_c is the form factor drag coefficient, Q_c is the interference factor of the part, $\frac{S_{wet,c}}{S_{ref}}$ is the wetted to reference area ratio, and the $C_{D,other}$ accounts for other drag that the aircraft produces. These values are summed to the n components of the aircraft which is denoted by c. Based on the assumption that the flow of the aircraft is turbulent, the contribution of flow-induced shear is shown in Eq. (10).

$$C_{f,turbulent} = \frac{0.455}{[\log(Re)]^{2.58}} \quad \text{Eq. (10)}$$

The form factor varies from the aircraft components such that it describes the drag due to pressure accumulation from the surface of the part. The fuselage is only considered necessary to determine the form factor as shown in Eq. (11). The Mach number of the flow, the location of the thickest point of the airfoil, maximum thickness to chord length ratio are sufficient to determine the resulting form factor as shown in Eq. (12). The document by Sholz provided estimates for the flow's interference factor which are used in the team's calculations.

$$FF_{E/W} = [1 + \frac{0.6}{x_t} \frac{t}{c} + 100(\frac{t}{c})^4] * [1.34M^{0.18}] \quad \text{Eq. (11)}$$

$$FF_F = 1 + \frac{60}{(l_f/d_f)^3} + \frac{(l_f/d_f)}{400} \quad \text{Eq. (12)}$$

The induced drag or the resultant drag produced by lift is known to be quadratically proportional to the lift coefficient. It is inversely related to the aspect ratio of the wing and the Oswald efficiency factor. The Sholz document shows that the Oswald efficiency factor relies on the wing's taper ratio, aspect ratio, thickness-to-chord length ratio, and the number of engines.

$$C_{D,i} = \frac{C_L^2}{\pi e AR} \quad \text{Eq. (13)}$$

$$e = \frac{1}{(1 + 0,12 M^6)[1 + 0,142 + f(\lambda)AR(\frac{10 t}{c})^{0,33} + \frac{0,1(3 N_e + 1)}{(4 + AR)^{0,8}}]} \quad \text{Eq. (14)}$$

The induced drag and total drag values are shown in **Figure 4.14**.

	Parameter	Mission	Fuselage	Wing	H. Stabilizer	V. Stabilizer	Total
C_{D0}	Zero-Lift Drag	M-1	0.0085729	0.0151948	0.00315617	0.00180547	0.0287293
	Coefficient	M-2	0.0080706	0.0141792	0.00293540	0.00161215	0.0268664
		M-3	0.0080706	0.0141792	0.00293540	0.0016	0.0268664
C_F	Turbulent	M-1	0.00379773	0.00541985	0.00613786	0.00586650	—
	Skin-Friction Drag	M-2	0.00357523	0.00502759	0.00570194	0.00546277	—
	Coefficient	M-3	0.00357523	0.00502759	0.00570194	0.00546277	—
FF_{F/E/W}	Form Factor	—	1.057510918	1.168144439	1.100625	1.100625	—
Q_c	Interference Factor	—	1	1.2	1.03	1.03	—

Figure 4.14 • Non-dimensional drag parameters for each component.

Continuing, the magnitude of induced drag– or the resultant drag created by the presence of lift– is known to be quadratically proportional to the lift coefficient; it also is inversely related to the aircraft wing's aspect ratio and the Oswald efficiency factor **Eq. (15)**. The document by Sholz suggests that the Oswald efficiency factor relies on the total number of engines and the wing's aspect ratio, taper ratio, and thickness-to-chord length ratio **Eq. (16)**.

$$C_{D,i} = \frac{C_L^2}{\pi e AR} \quad \text{Eq. (15)}$$

$$e = \frac{1}{(1 + 0,12 M^6)[1 + 0,142 + f(\lambda)AR(\frac{10 t}{c})^{0,33} + \frac{0,1(3 N_e + 1)}{(4 + AR)^{0,8}}]} \quad \text{Eq. (16)}$$

The induced and total drag coefficient values for each configuration are documented below in **Figure 4.15**.

Parameter	M-1	M-2	M-3	
e	Oswald Efficiency Factor	0.841	0.841	0.841
C_{D0}	Zero-lift Drag Coefficient	0.0287	0.0269	0.0269
C_{DI}	Induced Drag Coefficient	0.007	0.0037	0.0037
C_D	Total Drag Coefficient	0.0353	0.0334	0.0334

Figure 4.15 • Efficiency factor and drag coefficients for each mission.

Additionally, the RC jamming antenna is considered to be a part of the drag analysis. In the analysis of the antenna, the group used a coefficient of drag of 0.5 for the shape of the antenna. From **Eq. (17)**, the team found that the drag that the antenna produces is 1.33 lb.

$$C_d = \frac{D}{\frac{1}{2} \rho V^2 S} \quad \text{Eq. (17)}$$

4.6 Stability and Control Analysis

The stability of the plane is dependent on its tail characteristics. **Eq. (18)** describes the horizontal tail volume ratio with respect to the elevator area S_H , elevator lever arm l_h , wing area S_W , and mean aerodynamic chord MAC . The elevator lever arm is defined as the distance from the aerodynamic center of the tail to the center of gravity of the plane. This equation was ultimately used to determine the tail sizing for the plane.

$$C_H = \frac{S_H \cdot l_h}{S_W \cdot MAC} \quad \text{Eq. (18)}$$

The team calculated a tail volume ratio close to 1, to maximize both maneuverability and stability. The team also calculated the static margin and pitching moment of the plane. They estimated the neutral point to be located at 45% of the mean aerodynamic chord, as this is a typical value for conventional wing-and-tube designs. The center of gravity calculated in weight and balance (Section 5.4) for each mission was used to find the static margin of the airplane. With the center of gravity and neutral point determined, the static margin can be calculated using **Eq. (19)**, which describes the static margin with respect to neutral point NP , center of gravity CG , and mean aerodynamic chord MAC .

$$SM = \frac{NP - CG}{MAC} \quad \text{Eq. (19)}$$

From the equation, SM is the static margin, NP is the neutral point, CG is the center of gravity, and MAC is the mean aerodynamic chord of the wing. The static pressure measures the stability of the plane. Generally, commercial airplanes have a static margin of 10% to 20%. For our airplane, the static margin falls in between 10% and 13%. **Figure 4.16** shows the static margin with limits of 5% and 25% and the center of gravity with limits calculated based on the static margin limits for each of the three missions.

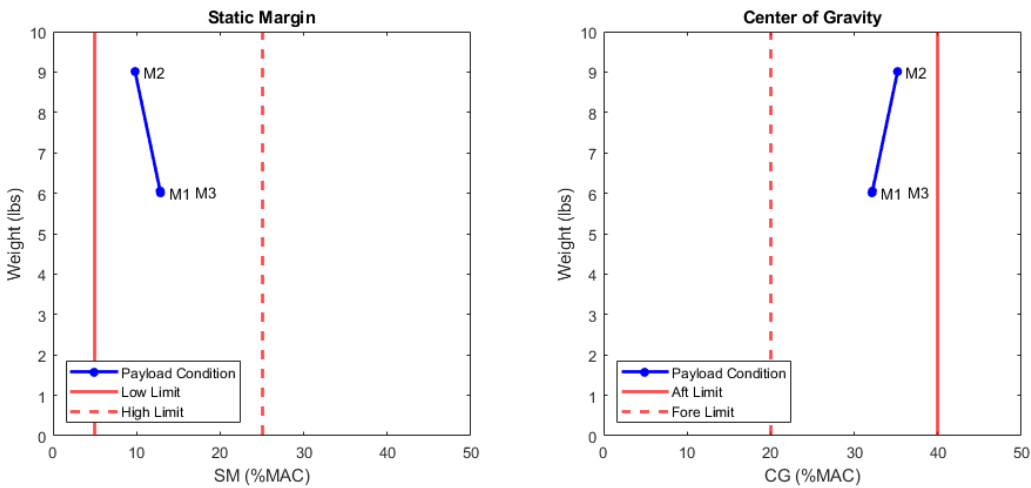


Figure 4.16: Static margin (left) and center of gravity (right) versus weight for each of the three mission load conditions.

4.7 Mission Model

DBF UCSD built upon MATLAB code and analyses from previous years in order to develop a mission model that provided a more accurate estimate of the aircraft's performance at the chosen and estimated parameters for each mission.

Based on user inputs of mass, maximum load factor, lift coefficient, wing surface area, etc., the team's flight simulation code first determines the velocity the aircraft will fly during the 1000 ft. long straights and the banked-angle turn portions of the course. From the combined velocity estimates, the code calculates the estimated flight time in which the aircraft will complete a single lap. A high-level overview of the code can be found in **Figure 4.17** below. The code allowed the team to develop estimates of the aircraft's performance, which are summarized in **Figure 4.18**.

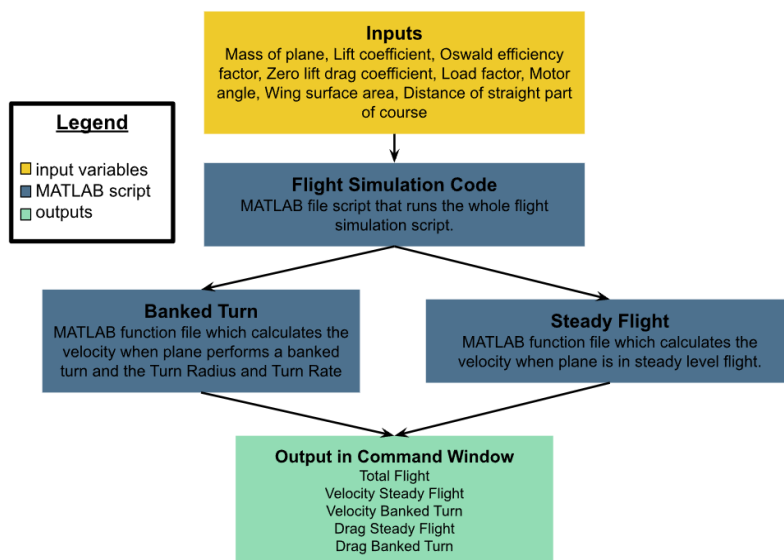


Figure 4.17 • Infographic which maps all of the inputs and outputs for the MATLAB scripts which simulate the aircraft performance while flying in the course.

Parameter	M-1	M-2	M-3
W_G	Takeoff weight 6.012 lb	9.012 lb	6.052 lb
v_{TO}	Takeoff velocity 40.01 ft/s	33.76 ft/s	39.56 ft/s
I_{CR}	Cruise power draw 13.5 A	14.6 A	13.5 A
T_{TF}	Endurance 12 min.	10.4 min.	12.0 min.
v_{SL}	Steady-level speed 53.62 ft/s	47.61 ft/s	53.61 ft/s
D_{SL}	Steady-level drag 0.028 lb	1.4 lb	1.4 lb
v_{BT}	Banked-turn speed 84.77 ft/s	67.57 ft/s	84.77 ft/s
D_{BT}	Banked-turn drag 0.044 lb	0.042 lb	0.042 lb
t_L	Lap time 25.9 s	34.01 s	25.9 s
E_L	Per-lap energy draw 97.13 mAh	137.92 mAh	97.13 mAh

Figure 4.18 • Model-generated estimated flight performance parameters.

Uncertainty from the model is due mainly to simplifying assumptions within the code. These include the assumptions that airspeed and thrust are constant and that no voltage decay occurs in the battery during the flight. Wind, pressure variation, and other complex external forces are neglected. Since the code was developed before the aircraft was constructed, it also draws upon assumptions and data collected in previous years that determined, among other things, maximum wing loading and climb angle. Finally, the model is unable to account for mid-flight pilot errors that may result in a suboptimal flight path or turning rate. The values in Figure 4.18 served as optimistic initial estimates to be verified or updated as additional testing data was obtained.

5. Detail Design

In the detail phase of the design process, DBF at UC San Diego finalized design decisions. They analyzed the structural capabilities and flight performance of their aircraft and determined the architecture of the sensor, its deployment mechanism, and other subsystems.

5.1 Final Design Parameters

Figures 5.1 and 5.2 summarize the aircraft's finalized dimensions, design characteristics, and electrical specifications.

Dimension	Fuselage	Wing	Horizontal stabilizer	Vertical stabilizer	Total
b or L	Span or length	25 in	54 in	22.3 in	10.8 in
H	Height	6 in	—	—	22.5 in
W	Width	6 in	—	—	78 in
C_{root}	Root chord	—	7.76 in	7.9 in	6.4 in
C_{tip}	Tip chord	—	7.76 in	7.9 in	6.4 in
MAC	Mean aerodynamic chord	—	7.76 in	6 in	6.75 in
S	Reference area	—	417.1 in ²	176.1 in ²	39.12 in ²
b²/S	Aspect ratio	—	6.96	2.82	1.69
Airfoil	NACA 2412				

Figure 5.1 • The aircraft's final dimensional characteristics. Values listed as applicable.

Tail servomotors	KST X08H	ESC	AVIAN SPMXAE 1080
Stall torque	73.6 oz.-in. at 8.4 V	Current rating	80.0 A
Servomotor speed	0.09 sec/60° at 8.4 V	Battery	Glacier 30C 6S
Servomotor weight	0.335 oz.	Number of cells	6
Wing servomotors	KST X10 Mini	Pack voltage	22.2 V
Stall torque	104.2 oz.-in. at 8.4 V	Pack weight	11.28 oz
Servomotor speed	0.09 sec/60° at 8.4 V	Motor	Scorpion SII-4025
Servomotor weight	0.811 oz.	Kv rating	420 Kv

Figure 5.2 • Electrical and mechanical specifications of the aircraft.

5.2 Structural characteristics

During flight and upon landing, the aircraft experiences different loads resulting from the wing and tail lift, the thrust of the motor, and reaction forces on the landing gears. **Figure 5.3** shows a free-body diagram of these forces. The DBF team analyzed the loads in the processes of making structural design choices for the aircraft, which are explained in detail in the following section.

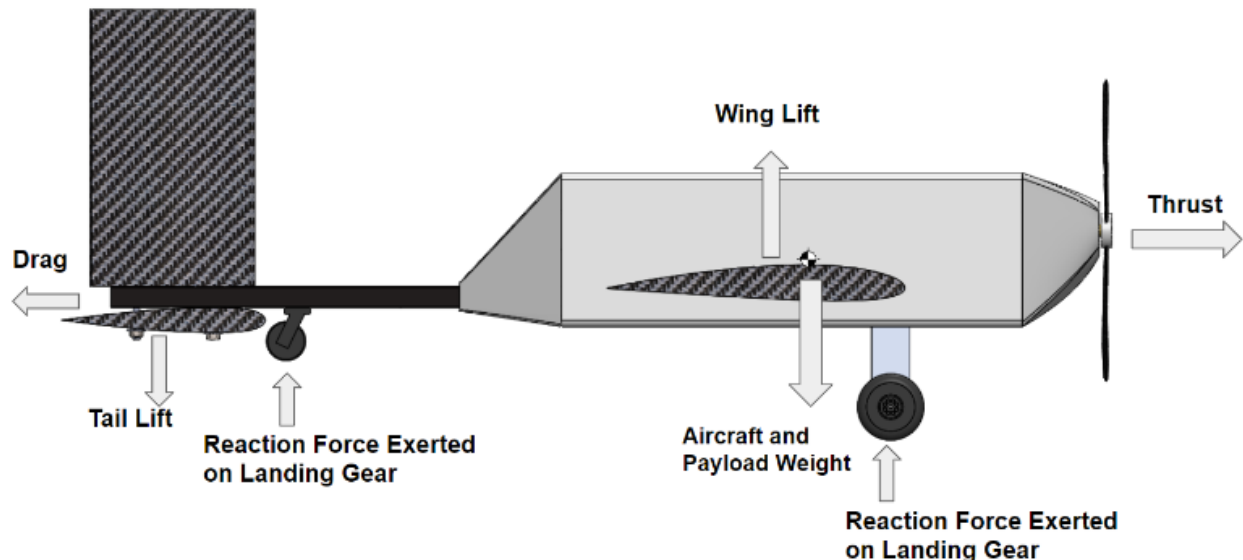


Figure 5.3 • Free body diagram of the aircraft

In addition to the external forces experienced on the aircraft, the team also conducted an analysis of the aerodynamic limits in which the plane can safely operate. The results determine that the aircraft can withstand a maximum of 2.5 positive load factor and a minimum load factor of -1.5. The V-n diagram together with a vertical gust envelope is shown in **Figure 5.4** and **Figure 5.5**. Since M2 and M3 have similar speed requirements, they are both represented in **Figure 5.5**.

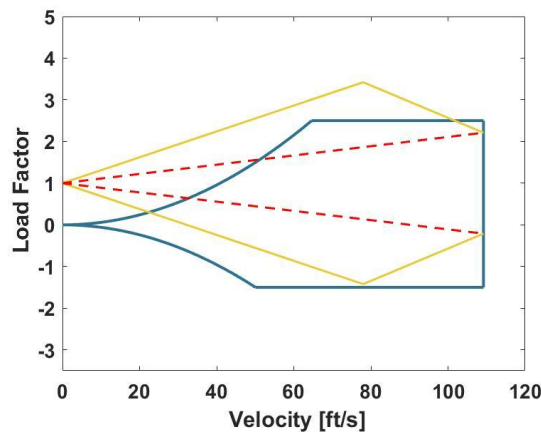


Figure 5.4 • V-n diagram for Mission 1

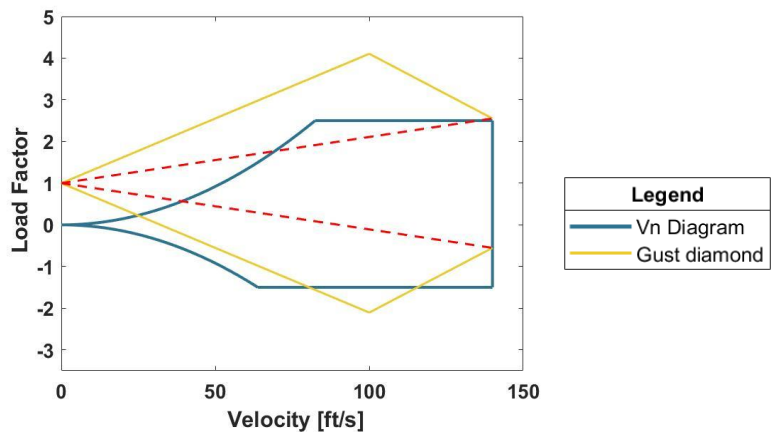


Figure 5.5 • V-n diagram for Missions 2 and 3.

5.3 System and subsystem architecture

The team designed the aircraft to best meet the mission requirements by investigating individual subsystems and their integration into the complete aircraft.

5.3.1 • Fuselage

The aircraft fuselage was designed to be as lightweight as possible with no moving parts inside of it. The team decided to employ a monocoque 1/8 in. balsa wood and plywood structure that is primarily constructed using glue, thereby minimizing complexity and weight. Due to time constraints, two-dimensional components were emphasized to allow for quick laser cutting and rapid prototyping. The wood frame fits in a bounding box that is 24 in. lengthwise, 5 in. widthwise, and 5 in. heightwise. The side plates are manufactured and designed as trusses to increase rigidity and spread loads evenly across different members. The lightening hole truss pattern of the side plates minimizes weight while the bottom plate has slots to ensure that the battery and electronics payload stay stable inside the fuselage during missions. Vertical columns placed along the length of the plane connect the top and bottom plates to transfer landing forces and provide torsional stability. A carbon fiber 0.75 in. X 0.83 in. boom that is fastened within the structure via M5 screws and inset T-nuts distributes vertical forces. Foam board skin throughout the fuselage and a nose cone and tail cone is used as an aerodynamic surface and for aerodynamic purposes. The foam board is attached permanently as it is epoxied to the wood fuselage framing. The usable cargo area of the fuselage is capable of holding 3 in. X 3 in. X 6 in. payload, as well as the battery, whose dimensions are 1.77 in. X 1.88 in. X 5.91 in. The payload is expected to weigh 30 percent of the total weight of the plane, and the battery weighs 0.32 lbs. Removable wing spars will be able to detach from the fuselage to allow the plane to fit into the competition storage requirements.

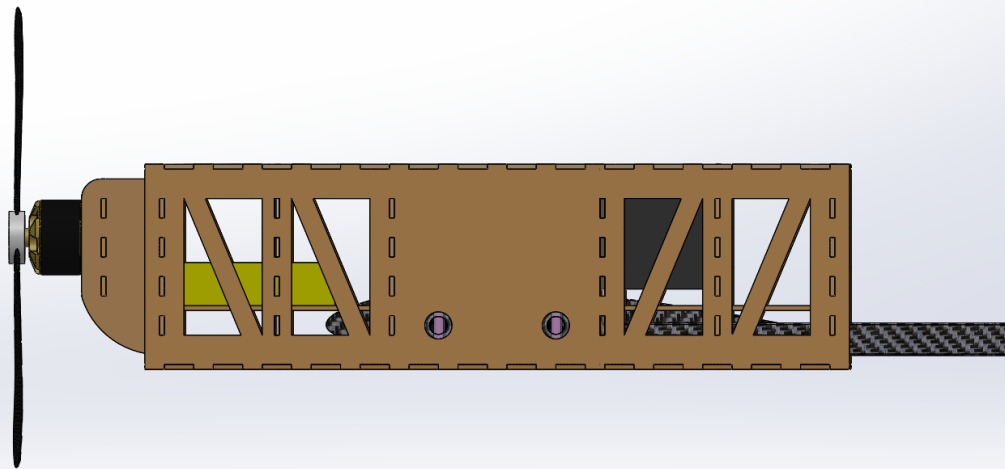


Figure 5.6 • Truss structure of Fuselage

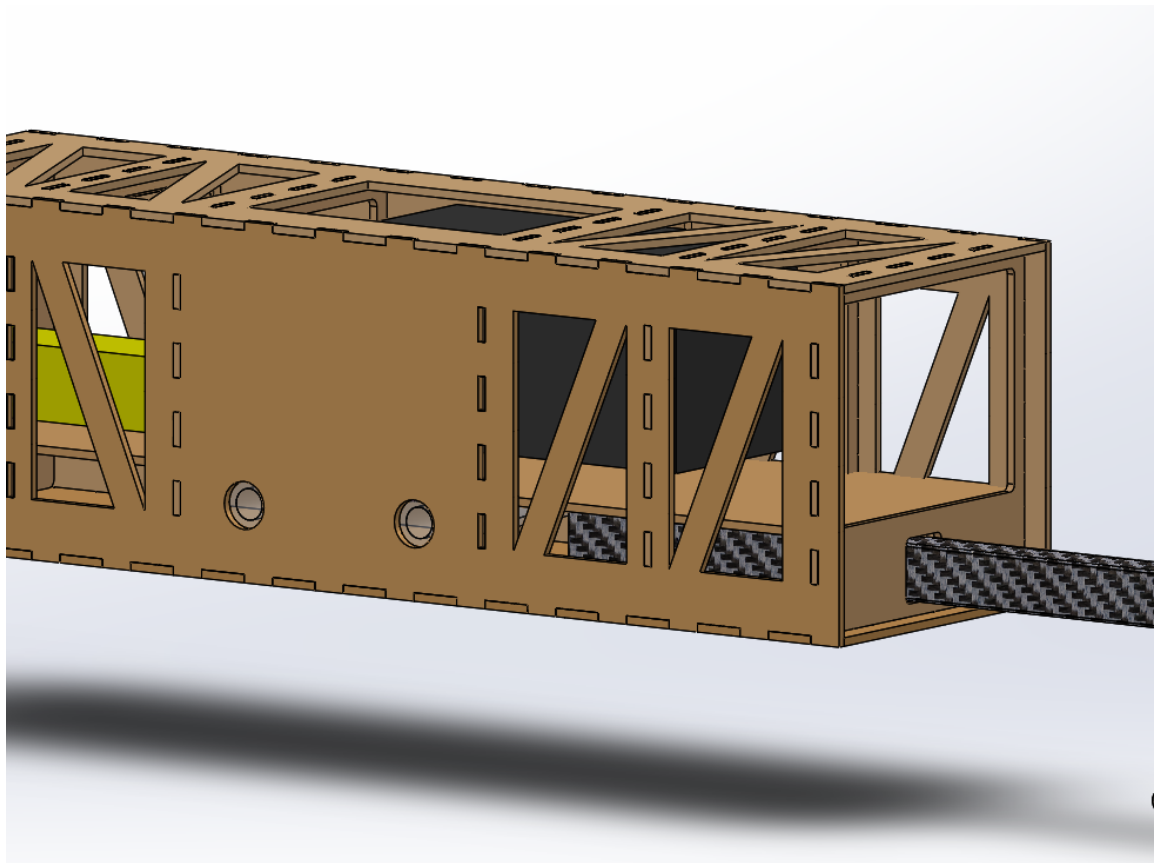


Figure 5.7 • Internal Fuselage Structure with boom attachment and payload

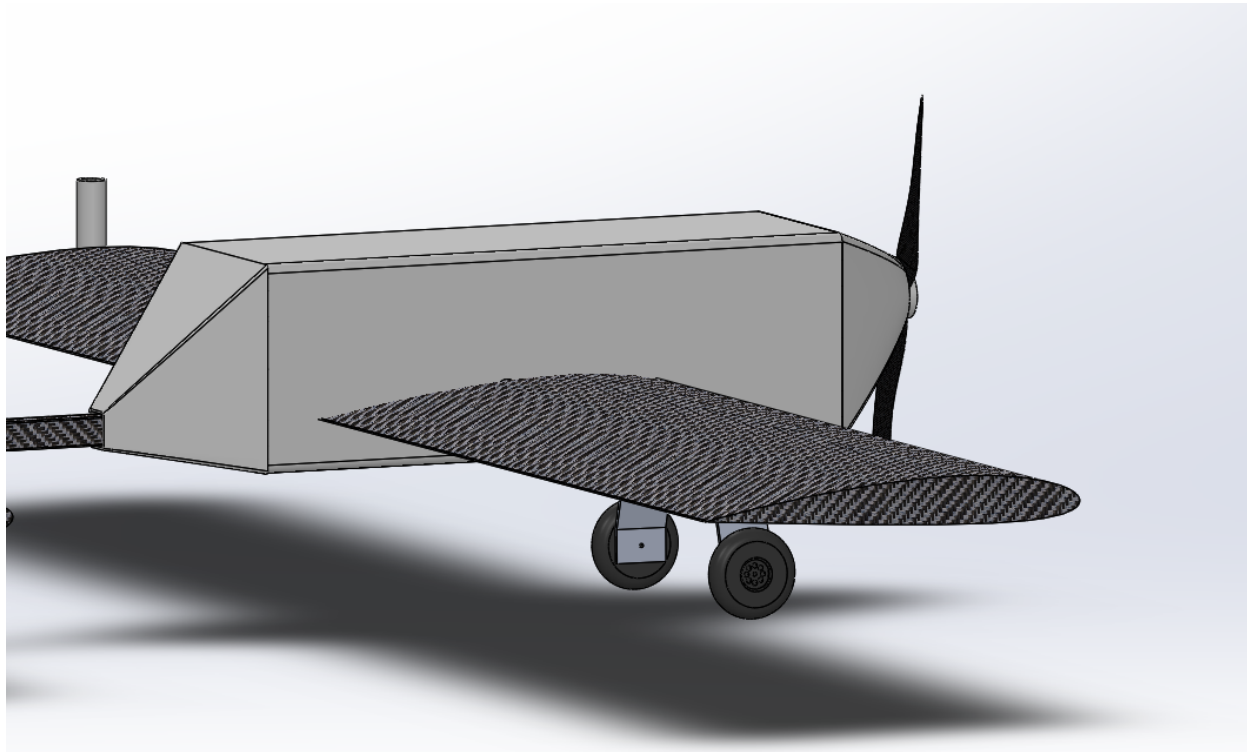


Figure 5.8 • Fuselage wrapped with foam skin

5.3.2 • Wing

The wing has a taper ratio of 1, and a wingspan of 54 in. It is made of foam and reinforced with carbon fiber. A mid-wing configuration was chosen to increase stability, ground clearance and reduce drag. The height of the wings allows for a secondary floor to be added within the fuselage to safely carry the payload and battery without interfering with the wing roots and attachments. The wings are detachable and connected to the fuselage with wing spars extending from the root. **Figure 5.10** shows the wing configuration. The spar from each wing half will be inserted into either side of a tube mounted inside the fuselage and fixed in place with a pin.

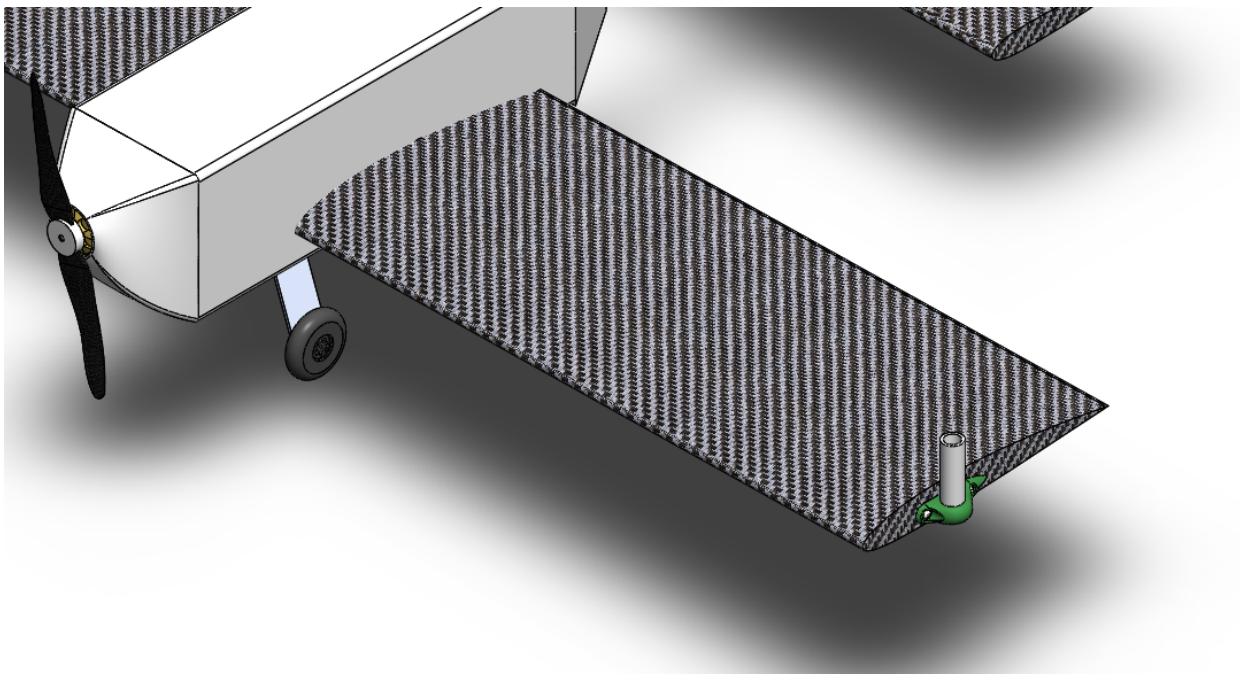


Figure 5.9 • Rectangular wing of the aircraft with antenna.

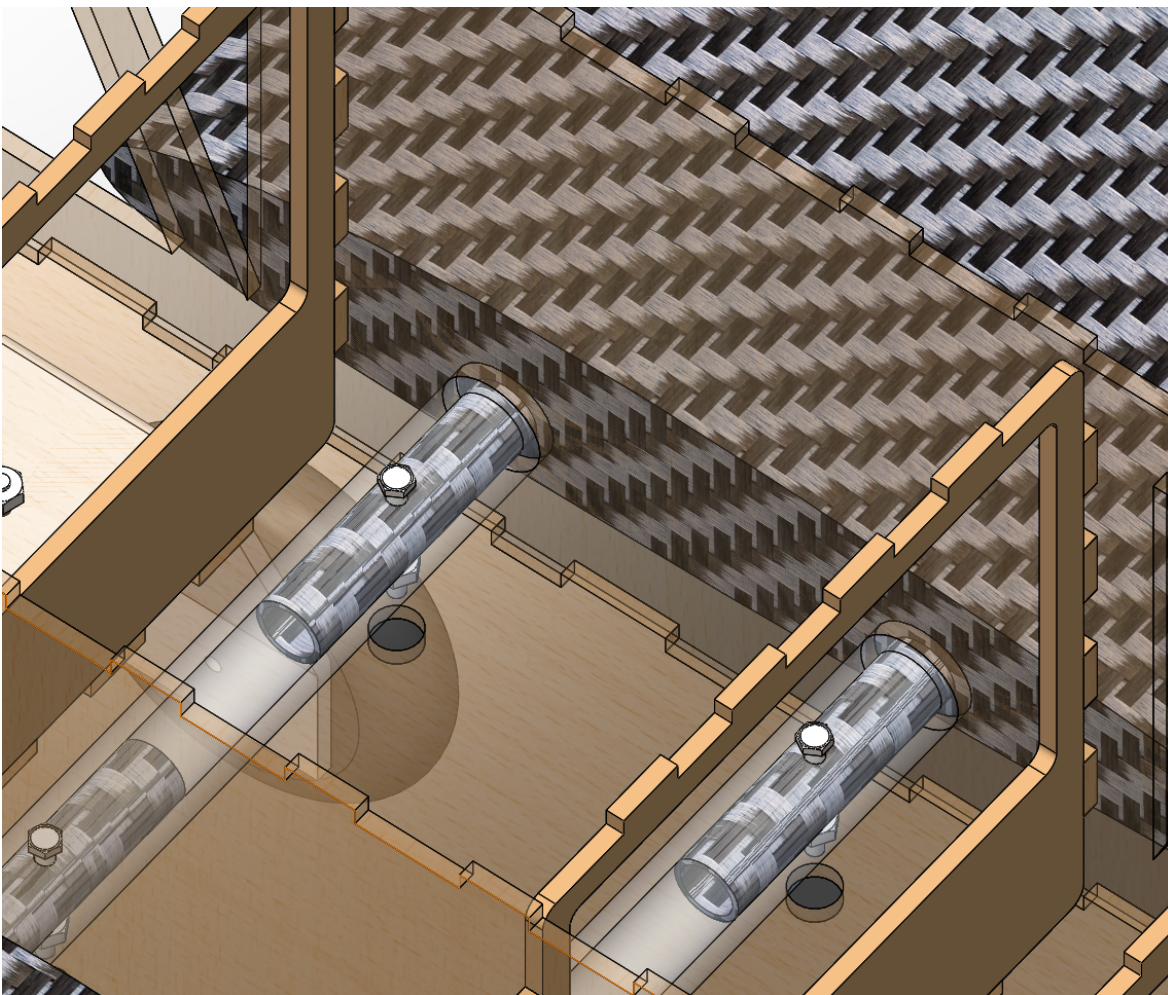


Figure 5.10 • Wing halves are attached to the fuselage via spar connectors.

5.3.3 • Empennage

The tail section has a rectangular horizontal stabilizer that is 22.3 in. x 7.9 in. dimensions, and a 10.8 in. high vertical stabilizer. They are manufactured using high-density foam and overlaid with carbon fiber for structural integrity. The team opted to use a conventional tail arrangement that would allow the stabilizers to be taken off and packed flat to minimize occupied volume. The vertical stabilizer will rest on top of the tail boom while the horizontal stabilizer is secured to the bottom of the boom. The vertical stabilizer will have threaded metal rods going through the carbon fiber boom located in the fuselage's tail and horizontal stabilizer with a nut and washer system to keep the separate pieces together (**Figure 5.11**). The metal rods enable the tail to withstand high-pressure forces during flight, as well as allow for a strong connection to the fuselage. The empennage is shown in **Figure 5.12**.

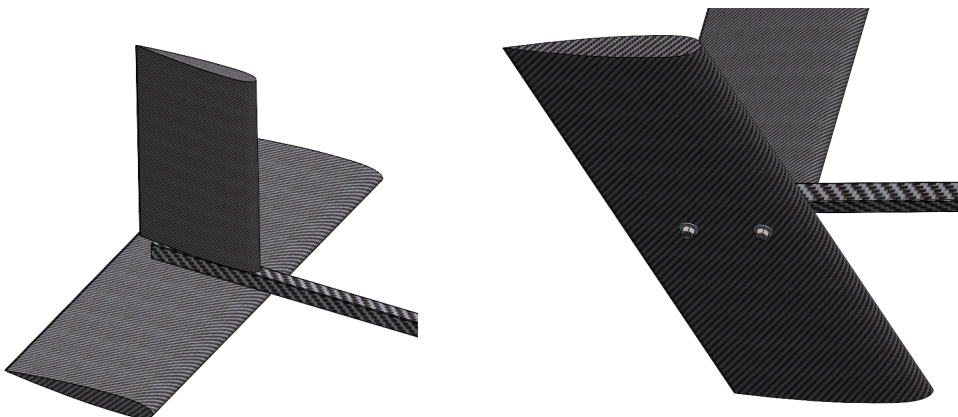


Figure 5.11 • The tail section of the aircraft.

Figure 5.12 • Empennage fasteners.

5.3.4 Landing Gear

The tail dragger landing gear is an easy configuration for smooth landing and take-off. It is also an optimal design consistent with a mid-wing aircraft. The main landing gear runs across the bottom of the fuselage, is mounted near a set of vertical columns, and measures 6 in. long with a 4 in. clearance above the ground (**Figure 5.13**). The height dimensions are chosen in order to have a center of gravity so the plane does not tip forward and the plane can produce a reduced amount of drag and pre-set angle of attack on takeoff.

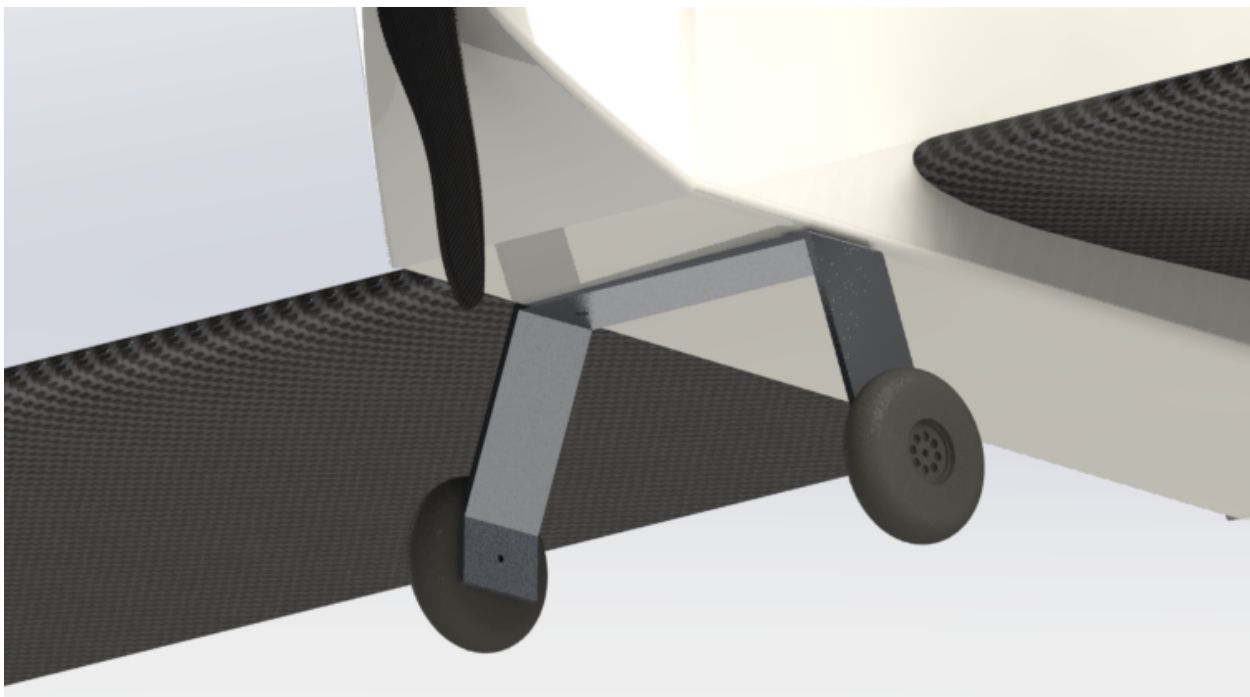


Figure 5.13 • Display of the main landing gear.

A finite element analysis using Von Mises simulation in Abaqus was conducted to determine the maximum load and displacement of the main landing gear. The analysis took into account a 1.5 Safety Factor when considering the load exerted on the landing gear. The results of the analysis are shown in **Figure 5.14** and in **Figure 5.15** with dimensions in units psi and inches, respectively. The yield strength was 2.1×10^4 psi.

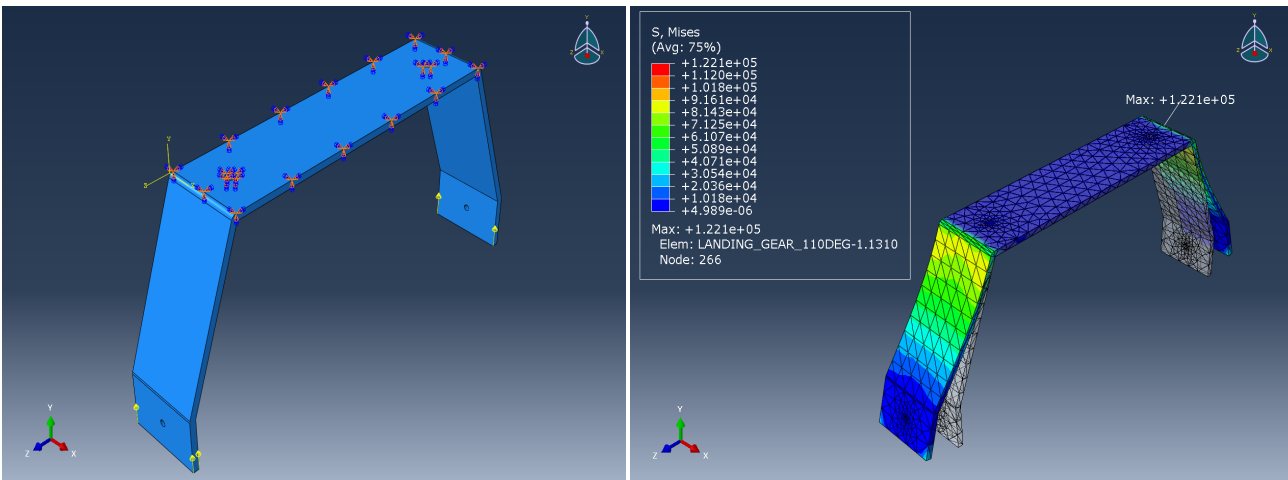


Figure 5.14 • Representation of the point of application of the forces exerted and the boundary conditions on the landing gear.

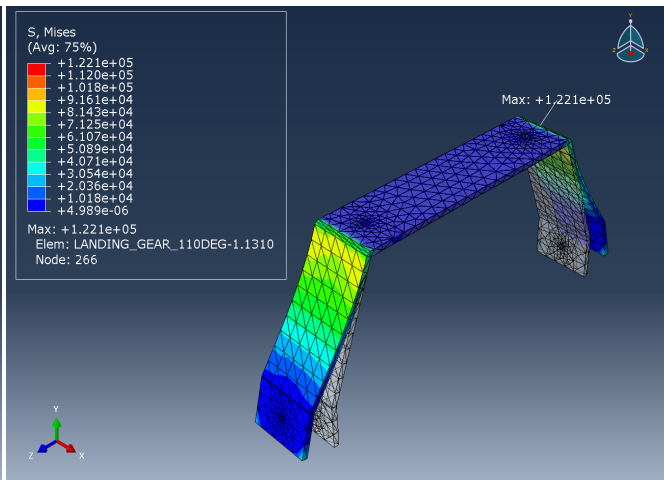
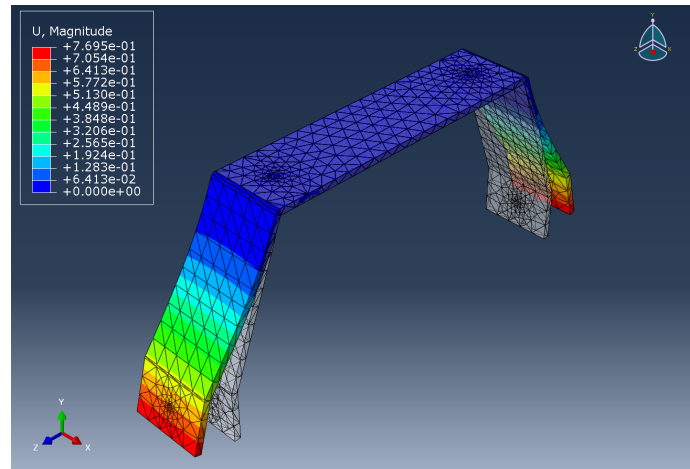


Figure 5.15 • Stresses in pounds per square inch experienced by the main landing gear.



. **Figure 5.16** • Displacement experienced at different locations of the landing gear during landings.

5.3.5 • Motor Mount

The structures team decided to create a wood structure motor mount that sits within the nose of the fuselage that uses a metal mounting bracket to bolt onto the plane. (**Figure 5.17**). It was found that attachment via screws on a screw plate and epoxy on the wood produced sufficient strength to support the motor. The carbon fiber skin on the wing was sanded to produce a rough surface to increase adhesion strength. The mount was designed to be wide enough to withstand the tensile and torsional forces.

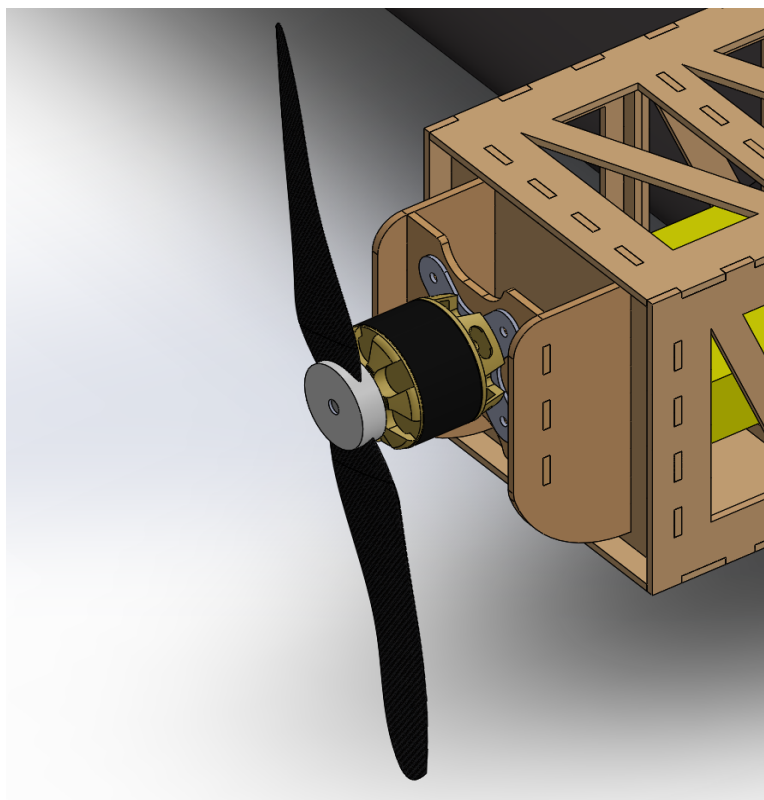


Figure 5.17 • Internal structure of motor mount with the motor and propeller attached to it.

5.3.7 • Avionics

The missions for this year are an electronic package and a jamming antenna. The design of the fuselage was the main focus of our team as it has to carry the payloads. It was built to carry an electronic package that is 30% of the gross vehicle weight, along with jamming antennas that are attached to the wing tip. The team decided to pair our Scorpion motor with the Spektrum Avian SPMXAE1080 Smart ESC to control the motors because of its superiority over ordinary ESCs. It can measure current, ESC temperature, motor speed, power consumption, voltage, and supports 3S to 8S LiPo batteries. It is also cooled with a large heatsink and fan. **Figure 5.18** compares the Smart ESC to a regular ESC.

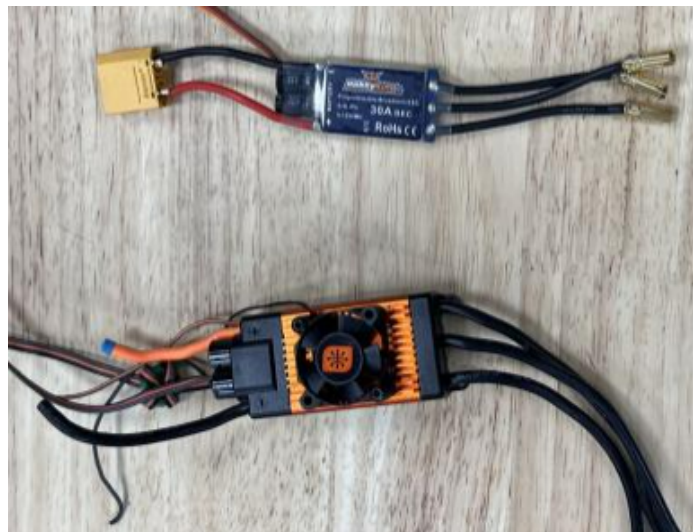


Figure 5.18 • A regular ESC vs an AVIAN SPMXAE 1080 Smart ESC.

5.4 Weight and balance

Figure 5.19 includes the plane's component weights and positions from the motor firewall toward the aircraft's rear (+X-direction) and below the thrust line (+Z-direction), along with the resultant weight and center of gravity positions for all configurations. Since the aircraft is symmetrical about the centerline, the distance along the Y-direction can be ignored.

Component and count	Case	Weight	X-distance	Z-distance
Battery	M-1	1.6 lb.	2.6621 in.	1.619 in.
	M-2	1.6 lb.	2.6621 in.	1.619 in.
	M-3	1.6 lb.	2.6621 in.	1.619 in.
Empennage	ALL	0.644 lb.	24.3031 in.	1.8857 in.
ESC	ALL	0.1 lb.	-0.5 in.	0.25 in.
Fuselage	ALL	0.48 lb.	8.0932 in.	1.541 in.
Landing gear	ALL	0.63 lb.	4.7508 in.	4.7565 in.
Motor	ALL	0.778 lb.	-2.4824 in.	0 in.
Receiver	ALL	0.03 lb.	0.126 in.	0.5 in.

Wing	$\times 1$	ALL	1.75 lb.	8.9871 in.	2.0688 in.
Electronics Package	$\times 1$	M-2	3 lb.	8.9054 in.	0 in.
Antenna and Adapter	$\times 1$	M-3	0.04 lb.	8.0432 in.	1.1939 in.
Total		M-1	6.012 lb.	7.90937 in.	1.2731 in.
		M-2	9.012 lb.	8.2595 in.	0.8179 in.
		M-3	6.052 lb.	7.9135 in.	1.2636 in.

Figure 5.19 • Weight and balance. Distances in the X-direction are measured from the motor firewall; distances in the Z-direction are measured from the thrust line.

5.5 Expected performance

The analyses performed in § 4 allowed the team to develop expectations for the aircraft's flight during cruise and banked flight. The team also implemented a new flight simulation in order to more accurately predict the aircraft's performance throughout the entire flight. The model, written in MATLAB, utilizes user-inputted data obtained from the earlier flight simulation code and other trade studies in order to describe the initial conditions of the aircraft and flight location. Then, using a detailed aerodynamic model and a fourth-order Runge-Kutta method to approximate changes in state, it simulates a full course lap. The code outputs a matrix containing relevant state variables including lift, drag, and velocity over the course of the flight. **Figure 5.20** provides an overview of the code.

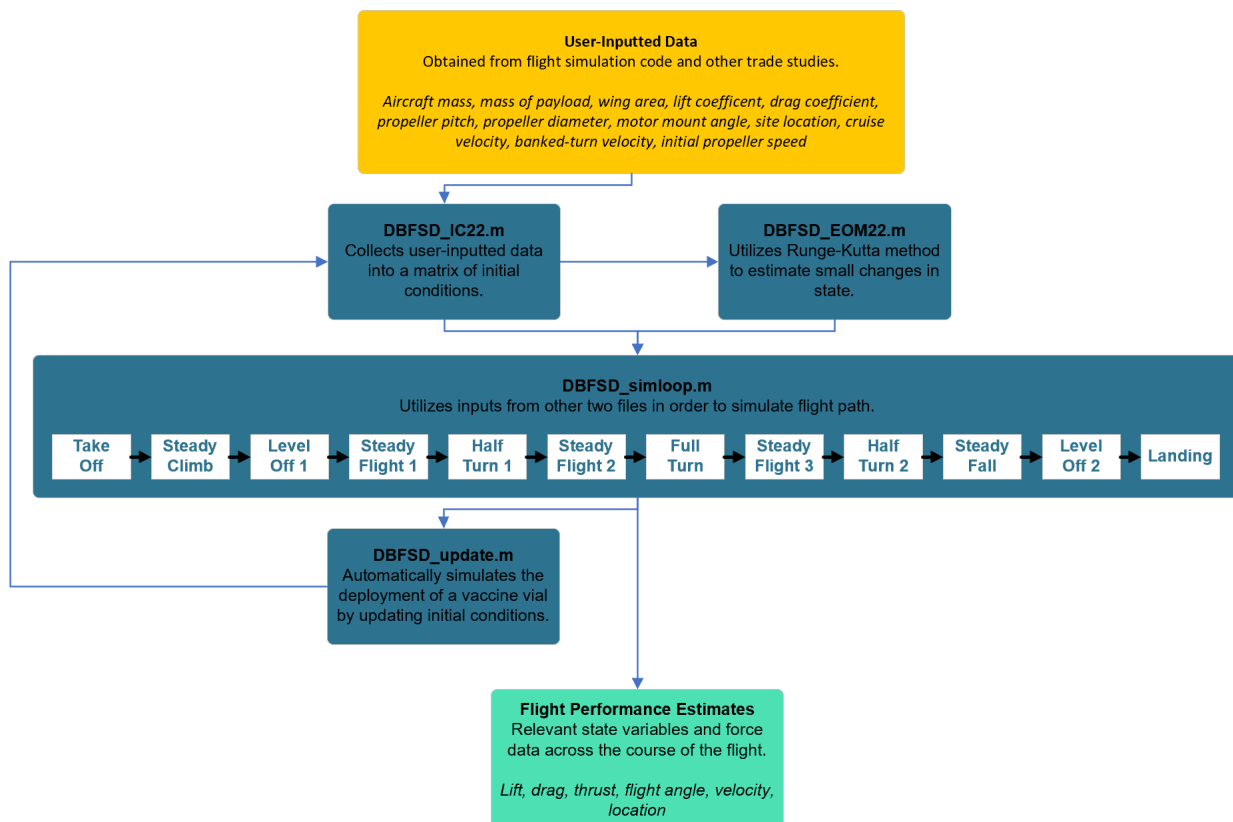


Figure 5.20 • A flowchart describing the components of the code used to estimate mission performance.

The expected flight performance metrics are summarized in **Figure 5.21**. This figure is similar to **Figure 4.18**, but values have been added and updated as necessary. **Figure 5.22** summarizes the expected mission performance of the aircraft. Values are derived from the MATLAB code as well as the sensitivity analysis, which factors in score distributions from previous years, along with a confident estimate of the team's relative performance, to generate a rough projected mission score.

Parameter	M-1	M-2	M-3
W_G	Takeoff weight 6.012 lb	9.012 lb	6.052 lb
v_{TO}	Takeoff velocity 56.12 ft/s	56.76 ft/s	56.17 ft/s
I_{CR}	Cruise power draw 12.5 A	13.8 A	12.5 A
T_{TF}	Endurance 12.4 min.	10.7 min.	12.4 min.
v_{SL}	Steady-level speed 49.67 ft/s	45.01 ft/s	49.65 ft/s
D_{SL}	Steady-level drag 0.028 lb	1.5 lb	1.5 lb
v_{BT}	Banked-turn speed 72.67 ft/s	67.57 ft/s	72.61 ft/s
D_{BT}	Banked-turn drag 0.045 lb	0.044 lb	0.044 lb
t_L	Lap time 25.9 s	34.01 s	25.9 s
E_L	Per-lap energy draw 98.13 mAh	111.91 mAh	98.14 mAh

Figure 5.21 • Model-generated estimated flight performance parameters.

Parameter	M-1	M-2	M-3
T	Lap time 36.7 s	45.8 s	37.8 s
x_{TOG}	Total Flight Time 110.1 s	137.4 s	113.4 s
nL	Number of laps 3	3	3
Sc	Projected mission score 1 of 1	1.2 of 2	2.3 of 3

Figure 5.22 • Model-generated estimated mission performance parameters.

5.6 • Drawing package

The following pages contain the drawing package for DBF at UC San Diego's 2021-22 fly-off aircraft.

6. Manufacturing Plan

The following section evaluates several manufacturing methods and materials to build the aircraft. It also describes the chosen assembly methods and outlines the team's manufacturing timeline.

6.1 Investigation of manufacturing processes

To find a production method that meets the design criteria of a high-performance and reliable aircraft and suits their current manufacturing capabilities, DBF at UC San Diego investigated multiple methods of production (**Figure 6.1**).

Methods	Advantages	Disadvantages
3D-printing	<ul style="list-style-type: none">- Low cost- Capable of making very complex parts- Parts can be quickly printed	<ul style="list-style-type: none">- Relatively fragile- Parts size restricted to printer size- Parts are isotropic
Balsa/Plywood	<ul style="list-style-type: none">- Low cost- Parts can be made expediently	<ul style="list-style-type: none">- Requires complex digital modeling to design
Carbon fiber composites	<ul style="list-style-type: none">- High stiffness-to-weight ratio- Lightweight	<ul style="list-style-type: none">- Expensive- Time-consuming layup process- Blocks certain frequencies of radio signals
Fiberglass composites	<ul style="list-style-type: none">- Does not block radio frequencies- High strength-to-weight ratio	<ul style="list-style-type: none">- Comparatively weaker than carbon fiber- Shrinks and distorts when wetted with epoxy resin- Soaks up more resin increasing weight
Foam-core structures	<ul style="list-style-type: none">- Can act as spacers to increase overall strength- Allows for quick prototyping	<ul style="list-style-type: none">- Requires sanding for a smooth surface
Hollow molded structures	<ul style="list-style-type: none">- Close resemblance to design profiles- Can be created using various materials	<ul style="list-style-type: none">- Time-consuming to fabricate the mold

Figure 6.1 • Production methods in consideration.

6.2 Assembly method selection

After assessing the production methods listed in **Figure 6.1**, the team optimized for assembly methods of specific components for the aircraft.

6.2.1 • Fuselage

The fuselage inner frame was chosen to be constructed out of $\frac{1}{8}$ inch balsa wood and plywood sheets. The team chose not to use composites due to a lack of time, experience, and monetary cost. The frame was chosen to have a box shape, with the outer layer providing a more aerodynamic shape. The internal parts would be laser cut, then glued together as joints. When the frame is assembled, the team would then cover the structure with foam board, adding structure and shape.

6.2.2 • Wing

The team used a hot-wire cutting CNC to cut the shape of the airfoil out of foam for manufacturing the wing (**Figure 6.2**). Using a handheld rotary bit tool, channels were cut into the wing, in which carbon fiber spars were laid for attachment and structural support.

For the composite layup, the team will apply epoxy to carbon fiber sheets on the foam core of the wing and then cover it with mylar to evenly distribute the epoxy along the wing's surface. To create moveable flaps and ailerons at the trailing edge of the wing, a section of the top surface of the trailing edge of the skin will be cut. Kevlar strips will be placed underneath the carbon fiber to reinforce the bottom wing skin below where the cut will be made. Gap-sealing tape will cover the control surfaces to add aerodynamic efficiency. Extra carbon fiber strips will be added to the leading edge of the wing for structural integrity. To ensure even distribution of the glue between the mylar and wing surface, the mylar, carbon, and epoxy-covered foam cores will be inserted into their respective molds they were cut out of and will be sealed in a vacuum bag. A vacuum pump will suck out all the air within the bag and press the two surfaces together to prevent voids from forming between the carbon fiber outer layer and foam core of the wing, preventing a weakening in the structural integrity of the wing.

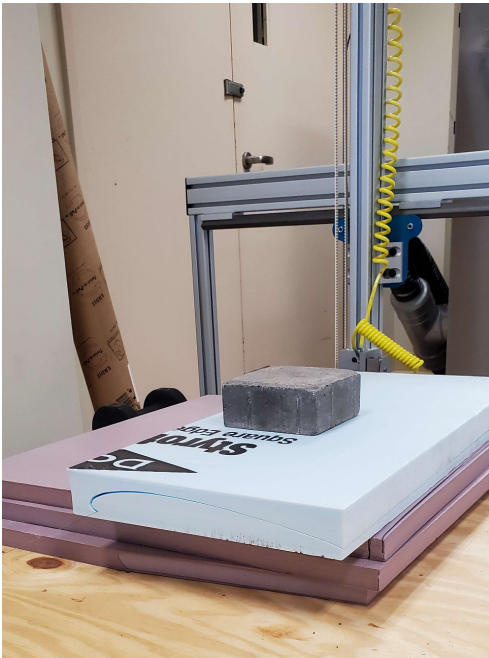


Figure 6.2 • The hot-wire cutter in the process of cutting out the foam wing.

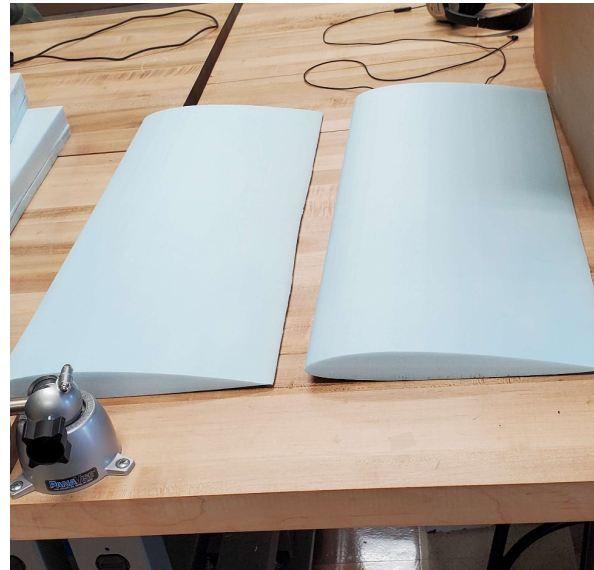


Figure 6.3 • Cut out wing halves displayed

6.2.3 • Tail

The tail was constructed in a similar process as the wing. Carbon fiber was overlaid over a foam core cut using a hot wire. In order to securely mount the tail components, the vertical tail section has two all-threaded rods inserted into it which fasten the vertical tail, the horizontal tail, and the carbon fiber boom to each other. Thin kevlar strings were tied at both ends of the vertical stabilizer to the fastened rods on the fuselage for tensioning and keeping the empennage intact. All control surfaces were covered with gap-covering tape and servos were covered with aerodynamic shrouds.

6.2.4 • Landing Gear

The landing gear was custom manufactured out of 1.5-inch wide and 1/8-inch thick aluminum bar stock. The bar was cut to length and two M5 holes were drilled that correspond to holes in the floor of the wood fuselage framing. It was then bent by 110 degrees on either side to form the legs. The tips of the legs were further bent to be vertical and holes were drilled to allow for the installation of wheels.

6.3 Manufacturing timeline

Due to the loss of an experienced team lead, and delayed manufacturing supplies, the fabrication process was immensely slowed down. Only one aircraft would be built for the 2022-23 contest season. This plane would serve as both the testing and competition plane.

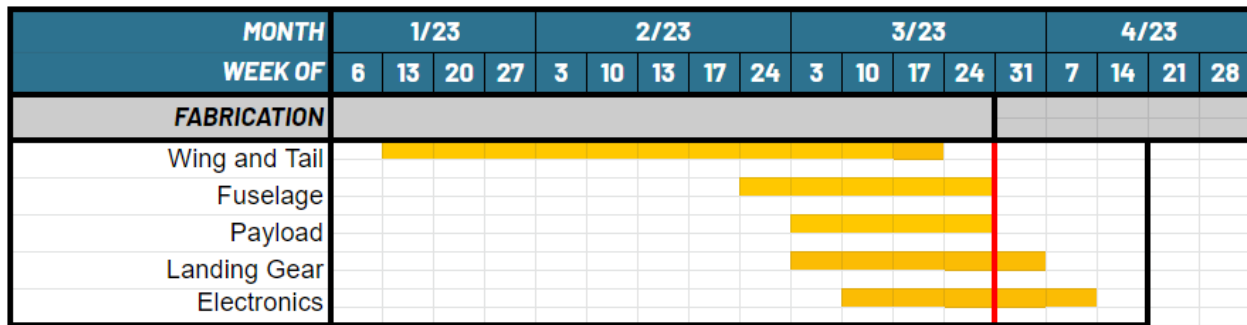


Figure 6.4 • A Gantt chart displaying the planned fabrication schedule.

7. Testing Plan

To gather flight data and optimize the performance of its competition aircraft, DBF at UC San Diego created a plan to test the aircraft's subsystems. This section discusses the team's comprehensive testing process.

7.1 Testing Schedule

The team has planned two test flights and various other subsystem tests throughout the 2022-23 competition season; the test schedule is shown in **Figure 7.1**. With the limited techniques and tools available to us, the team is in the process of conducting several tests on the aircraft's propulsion set-up, structural components, and other subsystems.

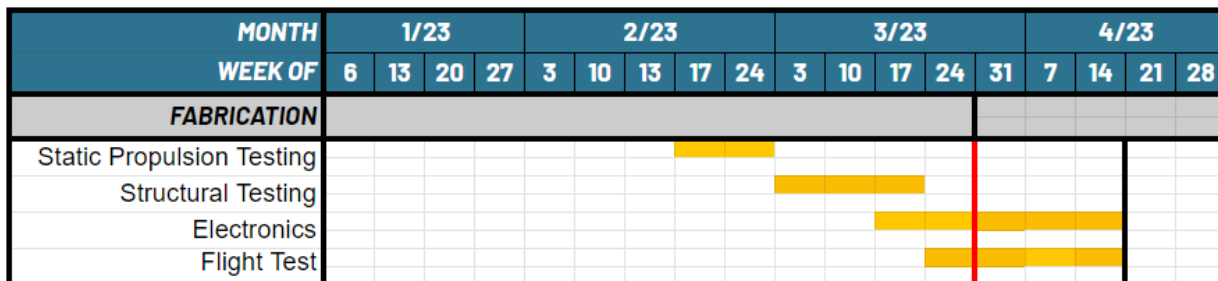


Figure 7.1 • A Gantt chart displaying the planned testing schedule.

7.2 Ground Testing

Comprehensive ground testing will be performed prior to the first flight test in order to reduce the possibility of damage to the aircraft or flight team. The scheduled, ongoing, and future tests are documented below.

7.2.1 • Static propulsion testing

The team used an RC Benchmark dynamometer to measure voltage, current draw, electric power, thrust, and torque of the motor and propeller configuration at the ideal thrust values to ensure that the motor performs comparably to theoretical calculations. **Figure 7.2** shows the setup of the test stand, which was clamped down onto a sturdy table and connected to a computer running the RC Benchmark software. Since the chosen motor arrived close to the due date of the report, the team did not have enough time to perform a full endurance test at the recommended thrust for each mission. Thus, it was decided that the team will run the motors at the recommended thrust and RPM values, which their Propeller-Motor Master Optimization Script outputted, for each mission over the duration of five minutes. The data recorded by the dynamometer were saved to a comma-separated value file and parsed and analyzed by a MATLAB script. The results and interpretation of this data can be found later in this report in section 8.1.1.



Figure 7.2 • Static propulsion test stand running with the chosen motor, propeller, and battery that are used in the set.

7.3 Flight Testing Plan

Progressive tests utilizing the different mission configurations will be performed until we reach the desired performance and comfort level for the pilot.

7.3.1 • Risk Reduction and Preflight Checklist

Given that the team only plans to manufacture a single aircraft, reducing the risk of a mid-flight failure or crash is of the utmost importance. Before flying the aircraft, the team and the pilot will be required to verify the conditions specified in **Figure 7.3** and receive signatures from the attending lead members and from our advisor.

Preflight Checklist			
Propulsion		Controls	
Propeller Direction?	<input type="checkbox"/>	Receiver Connection?	<input type="checkbox"/>
Propeller Secured?	<input type="checkbox"/>	Control Surfaces Responsive?	<input type="checkbox"/>
Wiring Secured?	<input type="checkbox"/>	Telemetry Software On?	<input type="checkbox"/>
Motor Mounted Properly?	<input type="checkbox"/>	Visual Inspection?	<input type="checkbox"/>
Batteries Charged?	<input type="checkbox"/>	Aircraft	
Battery Voltages +/- 3V?	<input type="checkbox"/>	CG Verified?	<input type="checkbox"/>
Receiver Pack Charged?	<input type="checkbox"/>	Wing bolts tight?	<input type="checkbox"/>
Receiver On?	<input type="checkbox"/>	Hatches Closed?	<input type="checkbox"/>
Connection Secured?	<input type="checkbox"/>	Landing Gear Tight?	<input type="checkbox"/>

Payload		Signatures	
Weight Verified?	<input type="checkbox"/>	Pilot	_____
Payload Secure?	<input type="checkbox"/>	Faculty Advisor	_____
	<input type="checkbox"/>	Project Manager	_____
	<input type="checkbox"/>	Date	_____

Figure 7.3 • List of safety checks performed prior to each test flight.

7.3.2 • Flight Testing Schedule

The team plans to perform 9 test flights over the course of 2 sessions (Figure 7.4). The first flights are to be performed on the 18th of March 2023. They will first test the propulsion system performance, structural integrity, and overall flight capabilities of the aircraft with no payload or antenna. This strategy will allow the team to find and fix unforeseen problems before performing further tests and allow for the team pilot to familiarize themselves with the aircraft.

Date and location			
18 March 2023	1	M-1	
San Diego, California	2	M-1	
	3	M-1	
	4	M-1	
	5	M-2	
	6	M-2	
1 April 2023	7	M-2	
San Diego, California	8	M-3	
	9	M-3	

Figure 7.4 • List of test flights.

During test flights, the team will collect telemetry data detailing the current draw and cruise speed. The team will also manually measure takeoff distance, lap time, and flight endurance. These values will serve as a final confirmation of the team's design choices and reveal the necessity for any final design adjustments, such as a decrease in payload or shifts in weight and balancing. The data will be cross-referenced with the values obtained in trade studies and analyses in order to understand why the divergences occurred and to improve the analyses' accuracy for future years. The team will also consult with the pilot, a DBF at UC San Diego alumnus with many years of R/C piloting experience, to implement changes that will improve the handling or performance of the aircraft.

8. Performance Results

The following section documents the results of the tests described in § 7.

8.1 Aircraft and Subsystem Performance

The results of the tests that the team has performed thus far are compiled below.

8.1.1 • Propulsion Testing

In order to estimate mission durations based only on 5-minute runtimes of the motor and propeller configuration at the recommended thrust, the data collected by the dynamometer for each mission was plotted over time and linearly fit in order to obtain the rate of voltage decay. Using the slope values of the linear fit, the team was able to estimate the mission duration for each mission as the voltage decreases from a fully charged voltage of 25 V to 22.2 V, in order to prevent severe battery degradation since 22.2V is the voltage of the selected LiPo battery. Ideally, multiple endurance tests, or running the propulsion system at the recommended thrust and RPM from a fully charged battery to empty, would be performed in order to find the mission duration. However, since the static propulsion test occurred very close to the deadline of the report due date, the static propulsion test was only run on one battery and within only a snapshot of 5 minutes. According to **Figure 8.1**, the estimated mission duration for Mission 1 is 100 minutes, Mission 2 is 58.3 minutes, and Mission 3 is 53.3 minutes.

$$\text{mission duration} = \frac{V_{stop} - V_{start}}{V_{decay}} \quad \text{Eq (20)}$$

Figure 8.1 shows the recommended thrust and RPM, the calculated rate of voltage decay, and estimated mission durations.

Mission	Recommended Thrust	Voltage Range	Rate of Voltage Decay (Slope)	Estimated Mission Duration	Recommended RPM
M1	0.336 lbf	25-22.2 V	$- 4.7165 \times 10^{-4}$	6000 s.	6000 RPM
M2	0.413 lbf	25-22.2 V	$- 7.9946 \times 10^{-4}$	3500 s.	5000 RPM
M3	0.336 lbf	25-22.2 V	$- 9.075 \times 10^{-4}$	3200 s	5000 RPM

Figure 8.1 • Static motor test results.

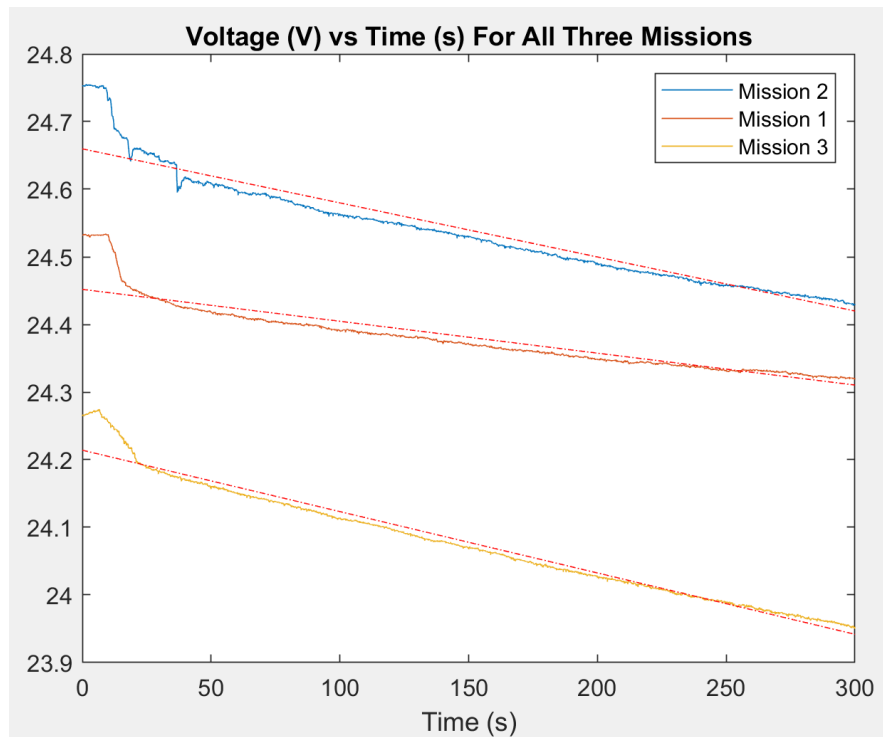


Figure 8.2: Voltage vs. Time plot of Mission 1, 2, and 3. The figure shows the decrease in voltage over time as the static propulsion test for each mission occurred. Each of these datasets was linearly fit (shown in red) to obtain the slopes of each dataset.

This year's last-minute static propulsion test revealed that the recommended thrust and airspeed values given to the propulsions subteam by the aerodynamics subteam might have been underestimated since the mission duration values occur to be much larger than reality flight duration regularly, which is around 10-20 minutes usually. In addition, the current draw for each mission, which is below 10 amps for all three missions, is far below the expected current draw of the propulsion system from last year, which was around 10 amps. Because of such subpar results, more experimental testing must be done to allow the team to verify that the propulsion system is adequate enough for keeping the aircraft flying and effectively satisfying the mission requirements. Because of this setback, the propulsion system chosen this year might not be the best propulsion system for our current plane.

To prevent this issue from occurring in the future, the team will explore new methods and workflows to obtain the estimated drag and recommended thrust for each mission, without the over-dependency between one subteam and another for input values, which may impact the accuracy of the MATLAB script used to select the most ideal propulsion system for the plane. The team will also consider ordering the components in a more timely manner so that there is ample time to perform the static propulsion testing. That way, the team will be able to use the results to catch any errors or flaws in the optimization process and prevent hindrances upon the selection of the most efficient propulsion system to tailor the team's aircraft to the mission requirements of the DBF competition.

8.2 Flight Performance

As described in § 2.4, DBF at UC San Diego was unable to access a majority of the fabrication materials until mid-February 2023 due to personnel change and subsequent delayed supply order. The team worked to make up for the lost time, but currently, only the wing and tail have been worked on. As a result, flight performance data is not yet available.

8.3 Future work and concluding remarks

In this report, DBF at UC San Diego documented our past, current, and future work to design, analyze, manufacture, and fly an aircraft at this year's Design/Build/Fly competition. The team went in with high hopes for this year's competition but encountered challenges that delayed the schedule similar to last year. There is a flaw in the organizational structure of the team, especially in the design process as seen in § 4.1, **Figure 4.1**. The fabrications subteam must wait on the design from aerodynamics, propulsions, and structures to finish their preliminary steps in order for supplies to be ordered. Another issue was the coupling of the aerodynamics and propulsion subteams. The current process of having the propulsion data use aerodynamics numbers creates a risk-prone model, in which mistakes in aerodynamics can lead to undetected bad data. In contrast, if the subteams were independent, it would make it easy for the data to be in conflict and examined.

Despite these organizational and logistical setbacks, the manufacturing process is currently making good progress. The team is confident that a competition plane will be built that can fly all three missions.

9. Bibliography

- [1] Hwang, J. T., Arnav V. J., and Tae H. H., ["Large-scale multidisciplinary design optimization—review and recommendations."](#) AIAA, San Diego, CA, June 2019.
- [2] Bunge, R., ["Motor/propeller performance analysis and estimation."](#) Stanford University, 8 April 2016.
- [3] ["Motors."](#) Scorpion.
- [4] ["Performance data,"](#) Advanced Precision Composites.
- [5] Scholz, D., ["Drag Prediction,"](#) Aircraft Design - an Open Educational Resource (OER) for Hamburg Open Online University (HOOU).
- [6] "Airfoil database search," retrieved 3 November 2021. <http://www.airfoiltools.com/>